

Dark matter and collider phenomenology of split-UED

This article has been downloaded from IOPscience. Please scroll down to see the full text article.

JHEP09(2009)078

(<http://iopscience.iop.org/1126-6708/2009/09/078>)

[The Table of Contents](#) and [more related content](#) is available

Download details:

IP Address: 80.92.225.132

The article was downloaded on 01/04/2010 at 13:42

Please note that [terms and conditions apply](#).

Dark matter and collider phenomenology of split-UED

Chuan-Ren Chen,^a Mihoko M. Nojiri,^{a,b,c} Seong Chan Park,^a Jing Shu^a and Michihisa Takeuchi^{b,d}

^a*Institute for the Physics and Mathematics of the Universe, The University of Tokyo, Kashiwa-no Ha, Kashiwa City, Chiba 277 – 8568, Japan*

^b*Theory Group, KEK*

1-1 Oho, Tsukuba, Ibaraki 305-0801, Japan

^c*The Graduate University for Advanced Studies (SOKENDAI),*

1-1 Oho, Tsukuba, Ibaraki 305-0801, Japan

^d*Yukawa Institute for Theoretical Physics, Kyoto University,*

Kyoto 606-8502, Japan

E-mail: chuan-ren.chen@ipmu.jp, nojiri@post.kek.jp,
seongchan.park@ipmu.jp, jing.shu@ipmu.jp,
M.Takeuchi@ThPhys.Uni-Heidelberg.de

ABSTRACT: We explicitly show that split-universal extra dimension (split-UED), a recently suggested extension of universal extra dimension (UED) model, can nicely explain recent anomalies in cosmic-ray positrons and electrons observed by PAMELA and ATIC/PPB-BETS. Kaluza-Klein (KK) dark matters mainly annihilate into leptons because the hadronic branching fraction is highly suppressed by large KK quark masses and the antiproton flux agrees very well with the observation where no excess is found. The flux of cosmic gamma-rays from pion decay is also highly suppressed and hardly detected in low energy region ($E_\gamma \lesssim 20$ GeV). Collider signatures of colored KK particles at the LHC, especially $q_1\bar{q}_1$ production, are studied in detail. Due to the large split in masses of KK quarks and other particles, hard p_T jets and missing E_T are generated, which make it possible to suppress the standard model background and discover the signals.

KEYWORDS: Phenomenology of Field Theories in Higher Dimensions

ARXIV EPRINT: [0903.1971](https://arxiv.org/abs/0903.1971)

Contents

1	Introduction	1
2	Masses and couplings in split-UED	3
3	Cosmic positron, antiproton and photon	7
3.1	Positron and electron	7
3.2	Antiproton	12
3.3	Gamma-ray	14
4	Collider signature of split-UED	16
5	Conclusion	20
6	Note added	21
A	KK decomposition in split-UED	22

1 Introduction

Recent observations by PAMELA [1] and ATIC/PPB-BETS [2, 3] consistently suggest a new primary source of energetic cosmic electrons and positrons in the neighborhood of our solar system, since high energy electrons/positrons lose their energy quickly within about 1 kpc. These results have attracted enormous attentions and stimulated many interpretations of the primary electric source from both astrophysics and particle physics, for example, the nearby pulsars [4] and dark matter decay [5] or annihilation [6]. The existing data of cosmic electrons and positrons cannot distinguish among these possibilities, and we expect that future data from cosmic-ray and accelerator experiments such as Fermi and Large Hadron Collider (LHC) will give us some clues on which interpretation is more promising and ultimately correct.

In this paper, we consider one of the most attractive models of dark matter, universal extra dimension (UED) with its minimal realization (mUED) [7, 8] and a recently suggested variety split-UED [9]. When the reflection symmetry (dubbed Kaluza-Klein parity) about the mid point of the orbifold extra dimension is exact, the lightest Kaluza-Klein particle (LKP), which is odd under the parity operation, is absolutely stable and is a good candidate of dark matter [10]. It turns out that in most cases of universal extra dimension scenarios the LKP is the first Kaluza-Klein (KK) photon (B_1), and a pair of charged leptons is produced in the annihilation process of B_1 . Interestingly enough, the mass of dark matter suggested by the ATIC/PPB-BETS data ($\sim 600 - 700$ GeV) exactly coincides with the

one that gives the right relic density for the LKP dark matter after taking co-annihilation channels into account [11].

On the other hand, the measured data of the cosmic ray antiproton-to-proton flux ratio between 1 and 100 GeV by PAMELA follow the expectations from secondary production and strongly constrain contributions from dark matter particle annihilation [12]. Therefore it is required to naturally reduce antiproton flux in any dark matter model. Split-UED is promising in the sense that production of antiproton is quite suppressed. The cross section for dark matter annihilates into a quark pair is

$$\langle \sigma_{B_1 B_1 \rightarrow q \bar{q} v} \rangle \propto m_{B_1}^2 / (m_{B_1}^2 + m_{q_1}^2)^2$$

where m_{B_1} and m_{q_1} are the masses of B_1 and the first KK quark (q_1), respectively, and it can be significantly suppressed by increasing the masses of KK quarks, i.e. splitting the KK quarks from other particles. However we should keep in mind that predictions of the observed antiprotons from dark matter annihilation can vary quite a lot for different adopted diffusion models as we will see later. As hadronic production is suppressed in split-UED, we would also expect much less production of cosmic gamma-ray whose main source is decay of pions. This prediction will be tested by forthcoming data from the Fermi experiment [13].

The split spectrum of Kaluza-Klein particles is realized by introducing a bulk mass term for quarks in split-UED keeping the KK parity exact [9].¹ One immediate consequence is that the 5D wave functions of quark fields are quasi-localized at the boundaries and induce violation of the translational symmetry along the extra dimension. Accordingly the KK number conservation is violated in the quark sector, and KK-even gauge bosons could directly couple to the zero mode quarks at the tree level, which is forbidden in mUED. KK-even bosons could be copiously produced at colliders and it is promising to discover them, for example, by the 2nd KK gluon resonance at the LHC [9]. Another consequence is the heavy KK quark decay to the SM quark and KK boson, which will generate harder jets with large missing momentum compared to that in mUED due to a large mass splitting between KK quarks and other KK particles. Such differences may give us some handle to tell split-UED apart from mUED at the LHC.

This paper is organized as follows. In section 2 we review split-UED and show how the spectrum and the interactions are modified compared with those in mUED. Note that the renormalization group (RG) running is taken into account in our spectrum calculation. We then calculate the annihilation cross section to leptons and quarks with varying “bulk mass parameter”, μ , which is the only new extra parameter in split-UED. In section 3, we estimate the signals of cosmic-ray positrons, electrons, and antiprotons from LKP dark matter annihilation in both mUED [15] and split-UED, and compare our predictions with recent experimental data. Moreover, the diffusive gamma-ray is studied as well. In section 4, we consider the productions of KK quarks and gluons at the LHC, and we also discuss the possibility of discovering these signals and mass reconstructions. We finally conclude our studies in section 5.

¹In warped geometry KK parity could be kept in a different way [14].

2 Masses and couplings in split-UED

Our set-up is based on the all SM fields are “universally” propagating in one extra dimension, which is compactified on an orbifold, S^1/Z_2 , with the boundary points $y = \pm L$ (the orbifold radius $R = 2L/\pi$). The extension we have introduced is an scalar background $\Phi(y)$ that couples to each colored Dirac fermions $\Psi_q(x^\mu, y)$ in the 5D bulk where the corresponding standard model quark field q (=SU(2) singlets u_R^c, d_R^c and doublet Q_L) resides on the chiral zero mode after orbifold projection. A common Yukawa coupling λ ($\equiv \lambda_{Q_L} = \lambda_{u_R^c} = \lambda_{d_R^c}$) is assumed for *all* quarks so that any further source of flavor violation beyond the CKM matrix is automatically avoided and the model becomes more predictive.² Here we neglect the family indices but one can easily extend the model to include more generations. Finally the 5D action is given by the form

$$S_{\text{split-UED}} = \int d^4x \int_{-L}^L dy \left[\mathcal{L}_{\text{mUED}} - \lambda \Phi(y) \bar{\Psi}_q(x, y) \Psi_q(x, y) \right], \quad (2.1)$$

where the summation runs for all quark fields q , and $\mathcal{L}_{\text{mUED}}$ contains the usual mUED terms.

If we choose an odd background profile $\Phi(-y) = -\Phi(y)$ under the inversion symmetry about the middle point $y = 0$, we can see that the KK parity, which transforms the fields as $\Phi(x, y) \rightarrow \Phi(x, -y)$, $\Psi_q(x, y) \rightarrow \pm \gamma_5 \Psi_q(x, -y)$, is still a good symmetry of the Lagrangian. For quantitative concreteness we consider the simplest mass profile which respects the requirement: $\lambda \langle \Phi(y) \rangle = \mu \epsilon(y)$, where μ is the bulk mass parameter and $\epsilon(y)$ is a step function defined as +1 for $0 < y < L$ and -1 for $-L < y < 0$. As ($\lambda \rightarrow 0$) or equivalently ($\mu \rightarrow 0$), split-UED is continuously reduced to mUED thus we call this limit as “mUED limit” below. For gauge bosons, scalars, and leptons (l), their KK decompositions are the same as those in mUED, while for quarks, their odd masses will affect the KK decompositions. The details of the all KK decompositions in eq. (2.1) are presented in appendix A. Notice that in the case of KK decomposition, we also label the KK parity in addition to the KK number $n = \{n^- (\text{n odd}), n^+ (\text{n even})\}$.

The tree level mass for the n -th KK fermion is given by

$$m_{q_n}^{\text{tree}} = \sqrt{\mu^2 + k_n^2}, \quad (2.2)$$

$$m_{l_n}^{\text{tree}} = n/R, \quad (2.3)$$

if we neglect their masses coming from electroweak symmetry breaking. Here k_n is determined by the boundary conditions which are given by:

$$k_{n^-} = -|\mu| \tan k_n L, \quad (2.4)$$

$$k_{n^+} = n/R. \quad (2.5)$$

We choose the minimal universal boundary conditions at the energy cutoff scale Λ that all boundary kinetic terms vanish,³ and the general expression for the one-loop correction to

²In general the Yukawa coupling can be assigned for any fermion field in the bulk and they can be different from each other.

³One can also consider the non-universal boundary conditions as an extension. See for example, ref. [16].

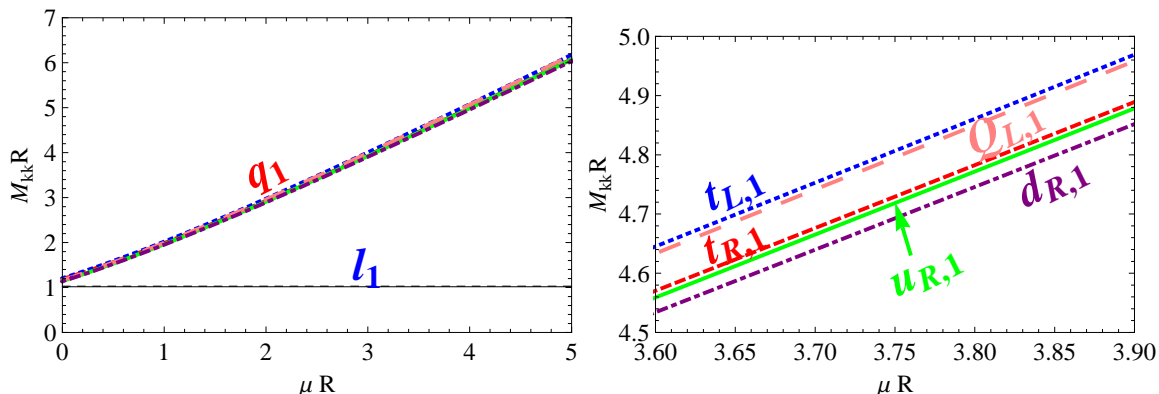


Figure 1. (upper plot) The spectra of 1st KK quarks and leptons in the unit $1/R$ with the given bulk mass parameter μ . The lepton masses are independent of μ in our scenario. Here we included 1-loop correction for all the masses. The most important correction is QCD correction and it is roughly $14 \sim 16\%$ for quarks. For leptons the correction is small ($\sim 2\%$). (lower plot) The magnified figure of the upper one in $\mu R = (3.60, 3.90)$. SU(2) doublets (t_L, Q_L) get the larger 1-loop correction than singlet quarks (u_R, d_R) get.

the n -th KK fermion masse is given by [17]

$$m_{f_n} = m_{f_n}^{\text{tree}} \left[1 + \frac{9}{8\pi} \left(\sum_G C_2^G(N) \alpha_G \right) \log \Lambda R \right], \quad (2.6)$$

where $\alpha_G = g_G^2/4\pi$ and we neglect the Yukawa corrections in this formula.⁴ The sum is over all SM gauge groups under which the fermion f is charged, and $C_2^G(N)$ is the quadratic Casimir operator of the fundamental representation N in gauge group G , e.g., $C_2^{\text{SU}(N)}(N) = (N^2 - 1)/2N$ and we take $C_2^{U(1)Y}(N) = Y_f^2$ with Y_f being the hypercharge of f . If we choose $(\alpha_1, \alpha_2, \alpha_3) \simeq (0.010, 0.033, 0.094)$ at $Q^2 = (620\text{GeV})^2$, colored particles will get bigger corrections ($\sim 14\%$ for u_R^1, d_R^1 and 16% for Q_L^1) than leptons ($\sim 1.9\%$ for l_R^1 and 3.1% for l_L^1). In figure 1 we plot the spectra of 1st KK quarks and leptons including 1-loop corrections. When $\mu = 0$, i.e. the mUED limit, quarks are quite degenerate with leptons even we take the QCD corrections to the masses into account. However when we increase the bulk mass parameter μ , the KK quark masses become larger and larger so that we get the split spectra as we request. Note that small deviations in quark spectra come from different SU(2) and U(1) charge of u_R, d_R and Q_L . In our study, these differences can be neglected.

The couplings between KK gauge bosons and fermions determine the most interesting phenomenological features of the model. All 4D effective couplings could be calculated by integrating out the 5D profiles of the relevant fields along the extra dimension. Since 5D profiles are the same for different KK gauge bosons (quarks) with the same KK number, the ratio between a general gauge boson-quark-quark coupling $g_{A_m - q_n - q'_l}$ over the SM one

⁴For the KK top quark, if we consider the large top Yukawa coupling, positive contribution to the tree level mass term will cancel the negative one from the radiative corrections, and the overall mass corrections will not be affected too much.

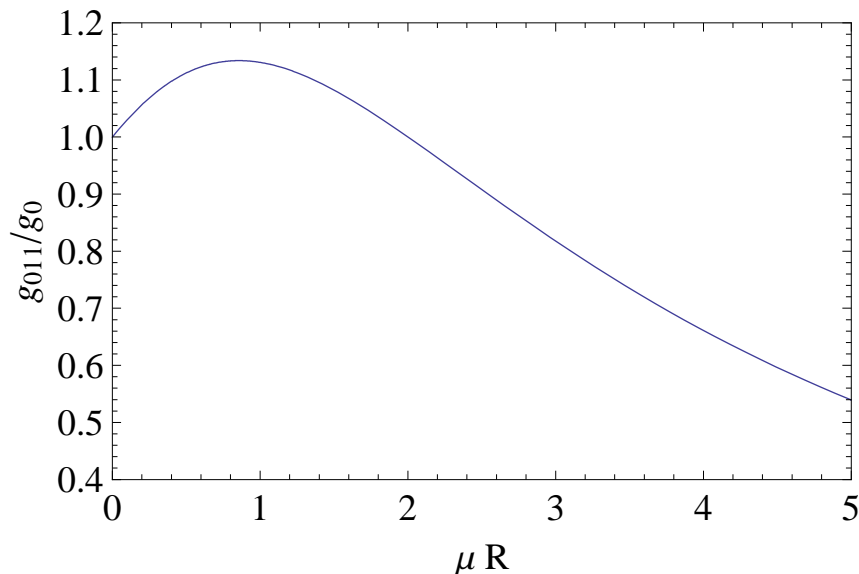


Figure 2. The coupling constant ratio $g_{A_1-q_1-q_0}/g_0 = \mathcal{G}_{110}$ versus μR . The dependence comes from the change of the 5D profiles. Notice that the coupling ratio first increases to its maximal value around 1.14 for $\mu R \sim 1$ and then decreases monotonically.

is the same for fixed KK numbers, where m , n and l are KK number of A , q and q' , respectively. We introduce a function $\mathcal{G}_{mnl}(\mu R)$ to parameterize how such a ratio depends on the bulk mass parameter μ times the radius R :

$$g_{A_m-q_n-q_l}/g_0 \equiv \mathcal{G}_{mnl}(\mu R), \tag{2.7}$$

where g_0 is the SM gauge interaction between A_0 , q_0 and q'_0 . Among those couplings, the most interesting one in phenomenology is the coupling between the 1st KK gauge boson A_1 , the 1st KK quark q_1 , and SM quark q_0 , which is crucial on LKP pair annihilation and productions of q_1 and the 1st KK gluon g_1 at the LHC. The dimensionless function $\mathcal{G}_{110}(\mu R)$ is calculated from the 5D profiles of A_1 , q_1 and q_0 given by eq. (A.1), (A.2), (A.3), and (A.5) in appendix A, and is plotted in figure 2 as a function of μR . At $\mu = 0$ limit we get the mUED result, which is the same as the SM coupling. As μ gets larger, the 5D profiles are localized so that the resultant overlap among the fields get smaller.

Taking care of all the corrections and effects of μ we can now calculate the branching fractions that LKP pair annihilates into quarks and leptons. At the non-relativistic limit ($\beta = \sqrt{1 - 4m_{B_1}^2/s} \rightarrow 0$), the cross section for LKP pair annihilates into fermions can be well approximated as:

$$\langle \sigma v \rangle_{B_1 B_1 \rightarrow f \bar{f}} = \frac{2g_1^4 C_f}{9\pi m_{B_1}^2} \left[\frac{\mathcal{G}_{110}(\mu R)}{(1+r_f^2)} \right]^2 + \mathcal{O}(v), \tag{2.8}$$

where a useful numerical term $C_f = N_c(Y_{fL}^4 + Y_{fR}^4)$ is introduced with the color factor $N_c = 3(1)$ for quarks(leptons). The mass ratio between the LKP and KK fermion is

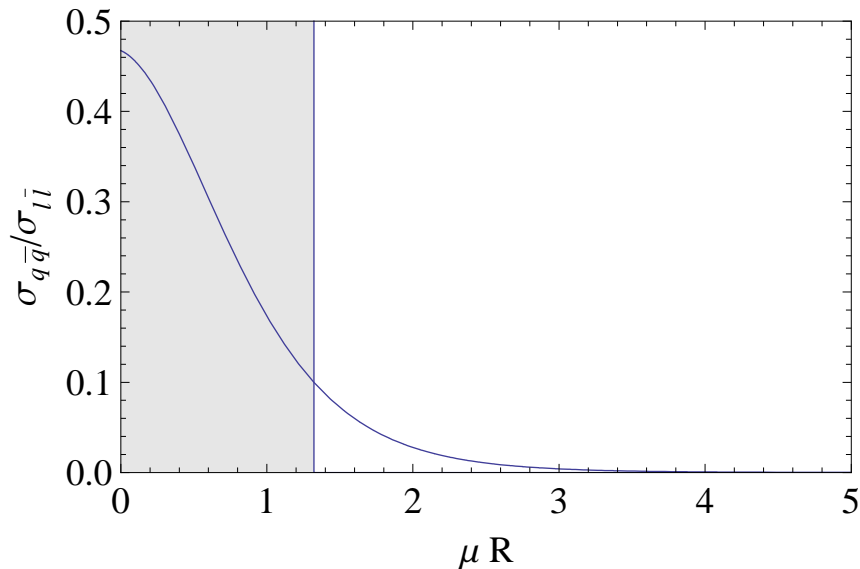


Figure 3. The ratio of LKP pair annihilation into quarks and charged leptons versus μR . The mUED limit corresponds to $\mu = 0$ and the ratio of cross section to quarks to leptons is about 47% but it quickly goes down below 10% as $\mu \gtrsim 1.3/R$. The shaded region ($\sigma_{q\bar{q}}/\sigma_{l\bar{l}} > 10\%$) is not preferred by PAMELA antiproton data.

μ (GeV)	0	200	400	600	800	1000
M_{q_1} (GeV)	713	863	1026	1198	1378	1566
$\text{BR}(B_1 B_1 \rightarrow q\bar{q})$	29.4%	26.4%	20.6%	14.3%	8.9%	5.2%
$\text{BR}(B_1 B_1 \rightarrow l\bar{l})$	64.3%	67.1%	72.3%	78.2%	83.0%	86.5%
$\text{BR}(B_1 B_1 \rightarrow \nu\bar{\nu})$	3.8%	3.9%	4.3%	4.6%	4.9%	5.1%
$\text{BR}(B_1 B_1 \rightarrow \phi\phi^*)$	2.3%	2.4%	2.6%	2.8%	3.0%	3.1%

Table 1. The branching fraction of the LKP pair annihilates into various final states, for different q_1 mass, and different bulk mass parameter μ . The numbers shown are summed over generations. We neglect the W -boson final state because the $SU(2)$ component of LKP is too small. Here we fix the LKP mass to be 620 GeV and include the radiative corrections to all the masses according to ref. [17].

parameterized by a parameter r_f defined as $r_f \equiv m_{f_1}/m_{B_1}$ and we ignore the small mass corrections coming from $SU(2)_L$, $U(1)_Y$ gauge group so that $m_{f_1} = m_{f_{L1}} \simeq m_{f_{R1}}$. In mUED limit, the ratio between productions of the lepton and the quark is mainly controlled by the ratio of C_f from the hypercharges and color factor of fermions. For leptons and quarks the corresponding terms are $\sum_l C_l \simeq 3.18$ and $\sum_q C_q \simeq 1.90$, respectively. Obviously the mUED does have a sizable hadronic annihilation channel and a carefully study of antiproton flux is important. In the case of split-UED, one can easily adjust r_q to suppress the hadronic annihilation cross section. In figure 3 we plot the ratio of annihilation cross section into quarks and charged leptons $\sigma_{q\bar{q}}/\sigma_{l\bar{l}}$ with μR in the range of (0, 5). We find the ratio goes down very quickly as the bulk mass parameter goes larger since $\sigma \sim 1/(1+r_f^2)^2$.

Model	δ	$K_0(\text{kpc}^2/\text{Myr})$	$L(\text{kpc})$
M2	0.55	0.00595	1
MED	0.70	0.0112	4
M1	0.46	0.0765	15

Table 2. The parameters in the diffusion models which are comparable with B/C and generate minimum (M2), median (MED) and maximal (M1) positron flux.

By turning on the bulk mass parameter we can easily avoid the antiproton excess in the cosmic ray detection experiments. We also note that the soft gamma-ray from decay of hadrons, especially from pions, is under control in this set-up.

3 Cosmic positron, antiproton and photon

LKP dark matter B_1 will mainly annihilate into a fermion pair while the W-boson and Higgs boson modes are suppressed, as shown in table 1. For the quark-pair final state, due to the QCD hadronization process, a bunch of hadrons will be produced and sequentially decay into positrons/electrons, protons/antiprotons, photons and neutrinos. Moreover, positrons and electrons also originate in the leptonic channels: muon and tau (also generate photons) decay and direct production in $B_1 B_1 \rightarrow e^+ e^-$ process. In our calculation, we use PYTHIA [18] for the simulation of the QCD hadronization and the decays of particles. Since these stable particles from the dark matter annihilation in our Galaxy will propagate to our solar system and be observed as cosmic-ray signals, we estimate the predictions from our model, the split-UED, and compared with experimental data in this section. Due to the fact that excesses were observed in the positron fraction in PAMELA [1] and the flux of electron plus positron in ATIC/PPB-BETS [2, 3] while the ratio of antiproton to proton, \bar{p}/p , is consistent with the astrophysical background, we first explain positron and electron data from the dark matter annihilation. Then base on the parameters set by fitting the ATIC/PPB-BETS and PAMELA data, we calculate the \bar{p}/p and photon flux. Since the W-boson and the Higgs boson productions are highly suppressed in UED models we are considering, we will not take into account their contributions in the following calculations.

3.1 Positron and electron

In this section, we calculate the cosmic-ray positrons and electrons from the $B_1 B_1$ annihilation which account for the PAMELA and ATIC/PPB-BETS data. Since the dark matter annihilation generates the same amount of electrons and positrons, we only show the formula for positron flux below. After being produced from the dark matter annihilation process, the positrons will propagate in the magnetic field of the Milky Way. Because the magnetic fields are tangled, the motion of the positron can be described by a diffusion equation. Neglecting the convection and annihilation in the disk, the steady state solution must satisfy

$$K(E) \nabla^2 f_{e^+}(E, \vec{r}) + \frac{\partial}{\partial E} [b(E) f_{e^+}(E, \vec{r})] + Q(E, \vec{r}) = 0, \quad (3.1)$$

where f_{e^+} is the number density of e^+ per unit kinetic energy, $K(E) = K_0(E/\text{GeV})^\delta$ is the diffusion coefficient, $b(E) = 10^{-16}(E/\text{GeV})^2$ is the rate of energy loss and $Q(E, \vec{r})$ is the source of producing e^+ . In the B_1 dark matter annihilation case,

$$Q(E, \vec{r}) = \frac{1}{2} \left(\frac{\rho(\vec{r})}{m_{B_1}} \right)^2 \sum_i \langle \sigma v \rangle_i \left(\frac{dN(E)_{e^+}}{dE} \right)_i, \quad (3.2)$$

where dN_{e^+}/dE is the energy spectrum of e^+ obtained by using PYTHIA, the index i runs over all quark and charged lepton pairs and $\rho(\vec{r})$ is the dark matter profile. In our numerical calculations, we adopt an overall boost factor B_F and the isothermal halo model [19] which is given as⁵

$$\rho_{\text{halo}}(\vec{r}) = \frac{\rho_0}{1 + (r/r_c)^2}, \quad (3.3)$$

where $r = |\vec{r}|$ is the distance from our Galactic center, $r_c = 3.5$ kpc and ρ_0 is the parameter that is adjusted to yield a dark matter local halo density of $0.3 \text{ GeV}/\text{cm}^3$ [19] in our solar system. Considering the diffusion zone of a cylinder with radius R and half-height L , the solution for the positron flux at the Earth can be written in a useful form [20]

$$\Phi_{e^+}^{DM}(E) = \frac{c}{4\pi} f_{e^+}(E, r_\odot), \quad (3.4)$$

where c is the speed of light,

$$f_{e^+}(E, r_\odot) = \int_E^{m_{B_1}} \frac{10^{16}}{E'^2} dE' \sum_{n,m=1}^{\infty} Q_{n,m}(E') J_0 \left(\frac{\zeta_n r_\odot}{R} \right) \sin \left(\frac{m\pi}{2} \right) \times \exp \left[\left[\left(\frac{m\pi}{2L} \right)^2 + \left(\frac{\zeta_n}{R} \right)^2 \right] X \right] \quad (3.5)$$

where $E^{(')}$ is the energy in a unit of GeV, J_0 is the zeroth-order of the first kind Bessel function, $r_\odot \sim 8.5$ kpc is the distance from Milky Way center to the Sun, ζ_n is the n -th zero of the function J_0 ,

$$X = \frac{K_0 \times 10^{16}}{\delta - 1} \left[E^{\delta-1} - E'^{\delta-1} \right] \quad (3.6)$$

and

$$Q_{n,m}(E) = \frac{2}{J_1(\zeta_n)^2 R^2 L} \int_0^R dr r J_0 \left(\frac{\zeta_n r}{R} \right) \int_{-L}^L dz \sin \left(\frac{m\pi z}{2L} (L - z) \right) Q(E, \vec{r}). \quad (3.7)$$

The J_1 in the eq. (3.7) is the first-order of the Bessel function and the parameters δ, K_0 are set in the simulations of diffusion models to coincide with the observed cosmic-ray data, especially the Boron to Carbon ratio (B/C) [21]. The values for different diffusion models we adopted are listed in table 2 [22].

In addition to e^\pm fluxes from dark matter annihilation, there exist secondary e^\pm fluxes from interactions between cosmic-rays and nuclei in the interstellar medium. We use the

⁵Effectively we are using $\rho^2(r) = B_F \rho_{\text{halo}}^2(r)$

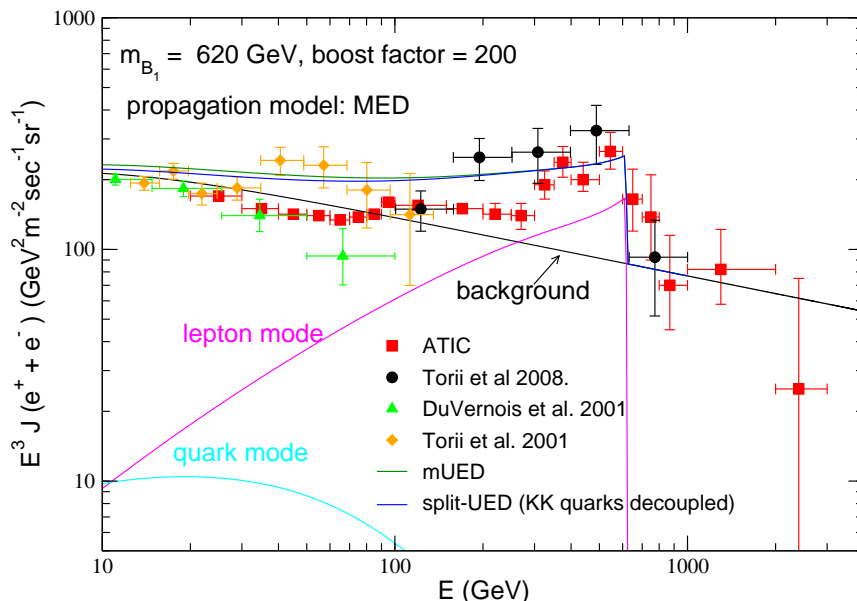


Figure 4. The flux of electron plus positron from LKP dark matter annihilation using MED diffusion model, compared with experimental data [2, 3, 26, 27]. Note that only lepton mode is included in the split-UED, since all the KK quarks are decoupled.

approximations of the e^- and e^+ background fluxes [23, 24]

$$\begin{aligned}\Phi_{e^-}^{prim}(E) &= \frac{0.16E^{-1.1}}{1 + 11E^{0.9} + 3.2E^{2.15}} \text{ GeV}^{-1}\text{cm}^{-2}\text{sec}^{-1}\text{sr}^{-1}, \\ \Phi_{e^-}^{sec}(E) &= \frac{0.7E^{0.7}}{1 + 110E^{1.5} + 600E^{2.9} + 580E^{4.2}} \text{ GeV}^{-1}\text{cm}^{-2}\text{sec}^{-1}\text{sr}^{-1}, \\ \Phi_{e^+}^{sec}(E) &= \frac{4.5E^{0.7}}{1 + 650E^{2.3} + 1500E^{4.2}} \text{ GeV}^{-1}\text{cm}^{-2}\text{sec}^{-1}\text{sr}^{-1},\end{aligned}\tag{3.8}$$

where E is in units of GeV. Therefore, the fraction of positron flux and total flux of positron plus electron are

$$\frac{\Phi_{e^+}^{DM} + \Phi_{e^+}^{sec}}{\Phi_{e^+}^{DM} + \Phi_{e^-}^{DM} + \Phi_{e^+}^{sec} + k\Phi_{e^-}^{prim} + \Phi_{e^-}^{sec}},\tag{3.9}$$

and

$$\Phi_{e^+}^{DM} + \Phi_{e^-}^{DM} + \Phi_{e^+}^{sec} + k\Phi_{e^-}^{prim} + \Phi_{e^-}^{sec},\tag{3.10}$$

respectively, where k is a free parameter which is used to fit the data when no primary source of e^+ flux exists [24, 25]. For our numerical simulation, we take the mass of dark matter, m_{B_1} to be 620 GeV. In figure 4, we show the total flux of electron and positron with the background from eq. (3.8) and recent experimental data [2, 3, 26, 27]. In order to have a better fit for the data, a boost factor of 200 is needed, which is consistent with the value (200) chosen in ref. [2]. Boost factor is known to have origins such as local clumps in dark matter profile [28] (see also [29]), Sommerfeld enhancement effect by a long range attractive force [30–34], the Breit-Wigner type resonance effect [35] and possibly many more origins. In our case, without assuming a new attractive force or further tuning of mass spectra to

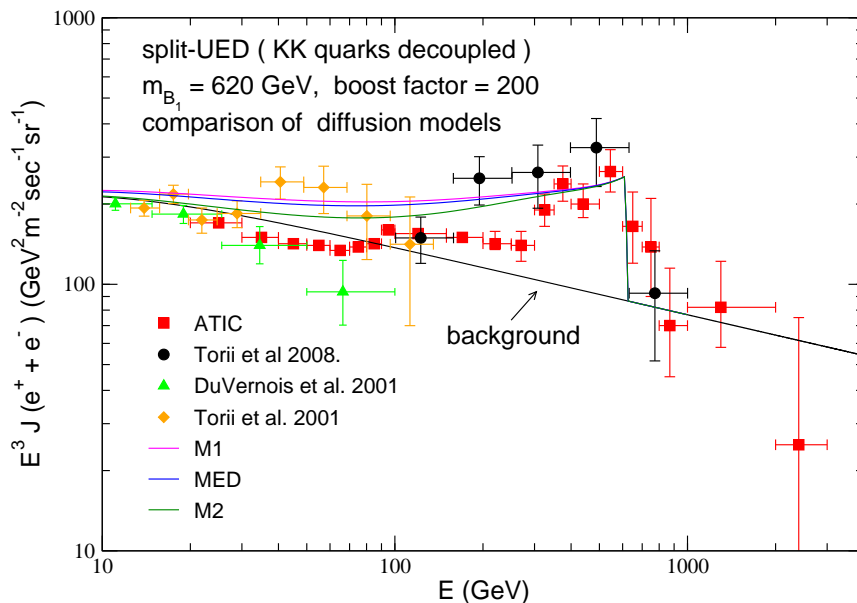


Figure 5. The same as figure 4 but only for split-UED, and different diffusion models, M1, MED and M2, are shown together.

get the large resonance, we tend to assume that boost factor mainly comes from clumps. We also show in figure 4 the contributions of quark mode and leptonic mode from the dark matter annihilation. The e^\pm from quark mode are much softer than that in the leptonic mode. This is because that the main source of e^\pm in quark mode is the hadron cascade decay while in leptonic mode there exists a direct production of $B_1 B_1 \rightarrow e^+ e^-$, and e^\pm from μ^\pm and τ^\pm decay are harder. We can easily see that the peak is mainly contributed by the leptonic mode and sharp drop-off is due to the direct production of e^\pm , therefore, the predictions of mUED and split-UED are quite similar to each other in the peak region since the difference between these two models is just in quark sector. We also compare different diffusion models in figure 5 for split-UED case. MED and M1 models produce more soft electrons and positrons than the M2 model does, thus the distributions of the former two models are flatter. For energetic positrons and electrons, all of three models are quite the same with each other. For positron fraction, we show in figure 6 the predictions of mUED and split-UED, using MED diffusion model, with PAMELA data [1]. Since there are more soft e^+ in mUED from the quark modes, the distribution is flatter compared to that of split-UED. If we adopt M2 and M1 models, as shown in figure 7, the fittings seem worse compared the MED case for split-UED especially in the energy region around 10 GeV. However, we have decoupled all of the higher KK quarks in this plot, i.e. hadronic final states are turned off in the dark matter annihilation. With finite mass of a first KK quark, more soft positrons will be produced, therefore, the M2 model can also be consistent with the data. For M1 model, we expect that by tuning the parameters, e.g. boost factor or the normalization of the background, it would be possible to explain the PAMELA data as well. So, we conclude here that the dark matter in both mUED and split-UED can be the equivalently good source of the excesses in PAMELA and ATIC/PPB-BETS data.

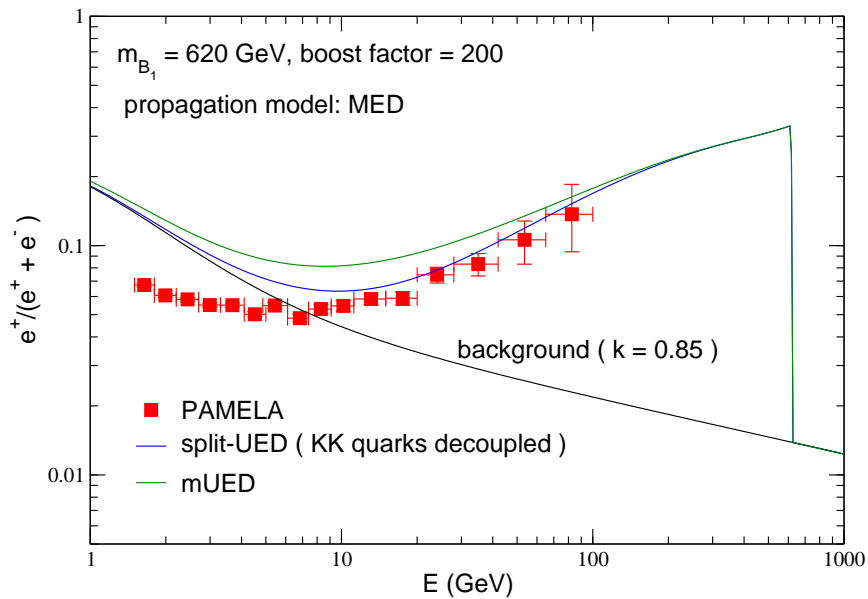


Figure 6. The positron flux fraction predicted from the LKP dark matter annihilation using MED diffusion model, compared with PAMELA data [1].

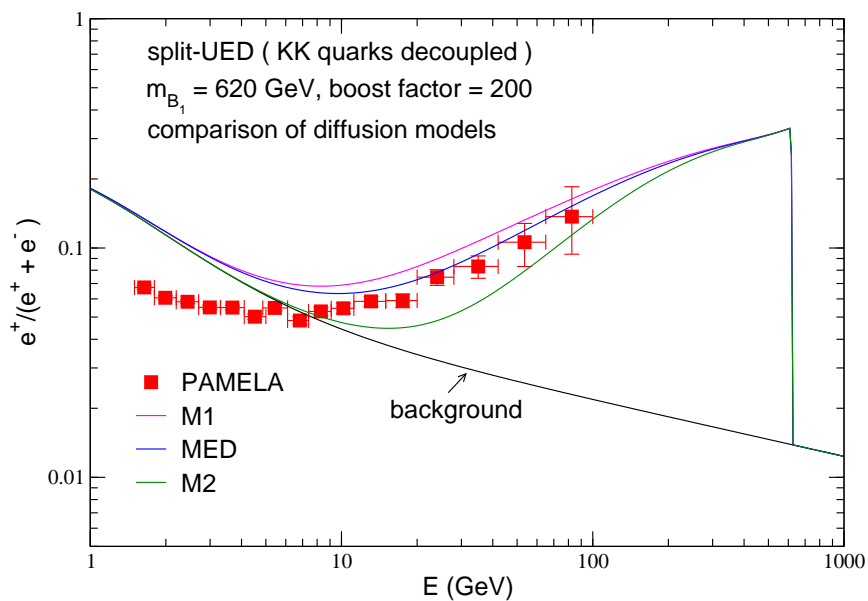


Figure 7. Same as figure 6 but only for split-UED, and different diffusion models, M1, MED and M2, are shown together.

3.2 Antiproton

The propagation of antiprotons through the Galaxy is similar to that of positrons. The diffusion equation of antiprotons can be described as

$$K_p \nabla^2 f_{\bar{p}}(T, \vec{r}) - \frac{\partial}{\partial z} [(sign\ of\ z) V_c(z) f_{\bar{p}}(T, \vec{r})] - 2h\delta(z)\Gamma_{ann} f_{\bar{p}}(T, \vec{r}) + Q(T, \vec{r}) = 0, \quad (3.11)$$

where $f_{\bar{p}}(T, \vec{r})$ is the number density of antiproton per unit energy, T is the kinetic energy of antiproton and $K_p = K_{0p}\beta(p/\text{GeV})^\delta$ is the diffusion parameter. $V_c(z)$ in the second term of eq. (3.11) is related to the convective wind that tends to push antiprotons away from the Galactic plane, and is assumed to be a constant. Again, like the case in positron, the values of K_{0p} , δ and V_c for different diffusion models are set to agree with the observed cosmic-ray data, especially the B/C, and their values are listed in table 3 [22]. The third term of eq. (3.11) represents the annihilation of \bar{p} with the interstellar proton in the Galactic plane, h is the half-height of plane which is set to be 0.1 kpc in our calculations. The antiproton annihilation rate Γ_{ann} is given as [36]

$$\Gamma_{ann} = (n_H + 4^{2/3}n_{He})\sigma_{\bar{p}p}^{ann}(T)v_{\bar{p}}, \quad (3.12)$$

where $n_H \sim 1/\text{cm}^3$ and $n_{He} \sim 0.07n_H$ are the number densities of hydrogen and helium, respectively; $\sigma_{\bar{p}p}^{ann}(T)$ is the annihilation cross section and $v_{\bar{p}}$ is the velocity of antiproton. The form of $\sigma_{\bar{p}p}^{ann}(T)$ is given by [37]

$$\sigma_{\bar{p}p}^{ann}(T) = \begin{cases} 661(1 + 0.0115T^{-0.774} - 0.948T^{0.0151}) \text{ mbarn} & , \text{ for } T < 15.5 \text{ GeV;} \\ 36T^{-0.5} \text{ mbarn} & , \text{ for } T \geq 15.5 \text{ GeV.} \end{cases} \quad (3.13)$$

The solution of the interstellar flux of antiproton in the vicinity of solar system is [38]

$$\begin{aligned} \Phi^{\text{IS}}(T) &= \frac{v_{\bar{p}}}{4\pi} f_{\bar{p}}(T, r_{\odot}^{\rightarrow}) \\ &= \frac{v_{\bar{p}}}{4\pi} \frac{1}{2m_{B_1}^2} \sum_i \langle \sigma v \rangle_i G(T) \left(\frac{dN_{\bar{p}}}{dT} \right)_i, \end{aligned} \quad (3.14)$$

where the $dN_{\bar{p}}/dT$ is the spectrum of antiproton which we simulate with PYTHIA, and the index i runs over all quark final states in the B_1 dark matter annihilation processes, and

$$G(T) = \sum_{n,m=1}^{\infty} J_0\left(\zeta_n \frac{r_{\odot}}{R}\right) \exp\left[-\frac{V_c L}{2K_p(T)}\right] \frac{y_n(L)}{A_n \sinh(S_n L/2)}, \quad (3.15)$$

with

$$y_n(L) = \frac{4}{J_1^2(\zeta_n) R^2} \int_0^R dr r J_0(\zeta_n r/R) \int_0^L dz \exp\left[\frac{V_c(L-z)}{2K_p(T)}\right] \sinh(S_n(L-z)/2) \rho(\vec{r})^2, \quad (3.16)$$

and

$$A_n = 2h\Gamma_{ann} + V_c + K_p(T)S_n \coth(S_n L/2), \quad (3.17)$$

$$S_n = \sqrt{\frac{V_c^2}{K_p^2(T)} + \frac{4\zeta_n^2}{R^2}}. \quad (3.18)$$

Model	δ	$K_{0p}(\text{kpc}^2/\text{Myr})$	$L(\text{kpc})$	$V_c(\text{km/s})$
MIN	0.85	0.0016	1	13.5
MED	0.70	0.0112	4	12
MAX	0.46	0.0765	15	5

Table 3. The parameters in the diffusion models which are comparable with B/C and generate minimum (MIN), median (MED) and maximal (MAX) antiproton flux.

However, we have to take solar modulation into account to estimate the flux of antiproton obtained at the the Earth, which is important for the low energy antiproton. The flux of the antiprotons at the top of Earth’s atmosphere can, therefore, be written as [39, 40]

$$\Phi_{\bar{p}}^{\text{TOA}}(T_{\text{TOA}}) = \frac{2m_p T_{\text{TOA}} + T_{\text{TOA}}^2}{2m_p T_{\text{IS}} + T_{\text{IS}}^2} \Phi_{\bar{p}}^{\text{IS}}(T_{\text{IS}}), \quad (3.19)$$

where $T_{\text{TOA}} = T_{\text{IS}} - \phi_F$ with ϕ_F being the solar modular parameter which we take to be 500 MV in our calculation. In order to compare with the observed data of antiproton to proton ratio, we need to include the astrophysical background. Here we adopt simple fittings for background antiprotons $\Phi_{\bar{p}}^{bg}$ and protons Φ_p^{bg} provided in ref. [41] ,

$$\Phi_{\bar{p}}^{bg} = \frac{0.9t^{-0.9}}{14 + 30t^{-1.85} + 0.08t^{2.3}} [\text{GeV}^{-1} \text{m}^{-2} \text{s}^{-1} \text{sr}^{-1}], \quad (3.20)$$

$$\Phi_p^{bg} = 10^4 \frac{0.9t^{-1}}{8 + 1.1t^{-1.85} + 0.8t^{1.68}} [\text{GeV}^{-1} \text{m}^{-2} \text{s}^{-1} \text{sr}^{-1}]. \quad (3.21)$$

The predicted ratios of antiproton to proton, \bar{p}/p , for mUED and split-UED are shown in figure 8 with experimental data [12, 42–45]. Here we take a common boost factor ($B_F = 200$) which we have obtained from ATIC/PPB-BETS fit. Since the hard electronic signals are mainly from local sources within a few kpcs but antiprotons can come from distant sources, one may take different values of boost factor for positron and antiproton in one’s calculation. Here, partly for predictability and simplicity and partly in order to follow common assumption that we live at a typical place in our galaxy, we take a common boost factor for all particles in our calculations. The mUED agrees well in the low energy region $E \lesssim 10 \text{ GeV}$, but starts deviating significantly from the recent PAMELA data when energy of antiproton becomes higher, if MED diffusion model is adopted. Therefore, mUED seems to be disfavored by PAMELA data in the high energy region, and it agrees with PAMELA observations only when MIN diffusion model is chosen. However, one can easily see that how the situation can be improved in the split-UED case. By enhancing the mass of q_1 to be twice of the l_1 , the prediction of \bar{p}/p is reduced by more than a factor of two, and will be much suppressed if q_1 becomes heavier, as shown by the blue and magenta lines in figure 8. We also note that if we adopt MIN model, the split-UED case agrees with PAMELA very well even for $m_{q_1} = 2m_{l_1}$. The lower bound of the mass of q_1 in split-UED can be estimated by the upcoming data of PAMELA in the higher energy region, since a small bump is predicted at $E \approx 200 \text{ GeV}$, and the height of deviation from background is controlled by the mass of q_1 .

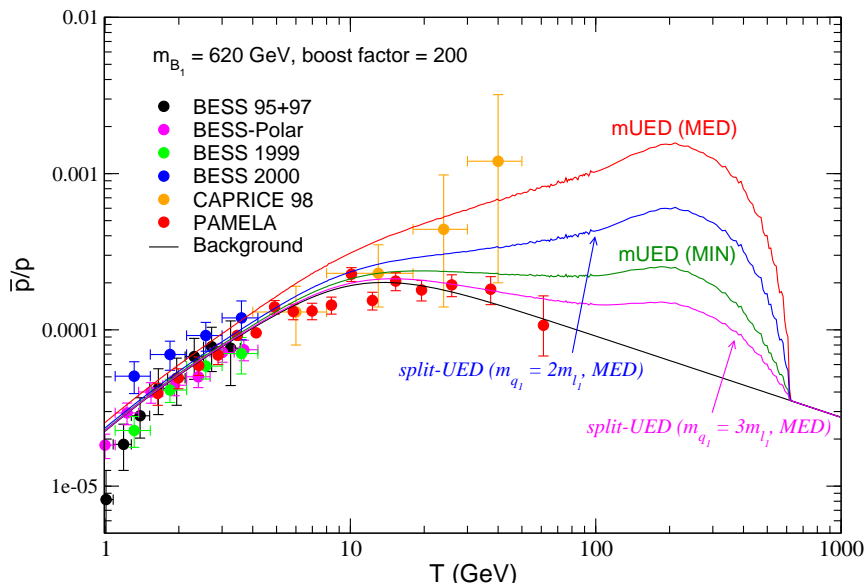


Figure 8. Antiproton to proton ratio predicted in mUED and split-UED models, together with experimental data. In mUED, both MED (red line) and MIN (green line) diffusion models are shown. For split-UED, the cases of $m_{q_1} = 2m_{l_1}$ (blue line) and $m_{q_1} = 3m_{l_1}$ (magenta line) are presented, using MED diffusion model.

3.3 Gamma-ray

For diffusive gamma-ray, there are galactic and extragalactic contributions from the annihilation of LKP dark matter B_1 . The flux of the gamma-ray from the extragalactic origin is estimated as [46]

$$\left[E^2 \frac{dJ_\gamma}{dE} \right]_{eg} = \frac{B_F E^2 c \Omega_{B_1}^2 \rho_c^2}{4\pi m_{B_1}^2 H_0 \Omega_M^{1/2}} \sum_i \langle \sigma v \rangle_i \int_0^{z_{up}} dy \left(\frac{dN_\gamma}{d((1+z)E)} \right)_i \frac{(1+z)^{-3/2} e^{-z/z_{max}}}{\sqrt{1 + \frac{\Omega_\Lambda}{\Omega_M} (1+z)^{-3}}}, \quad (3.22)$$

where Ω_{B_1} , Ω_M and Ω_Λ are the density parameters of B_1 , matter (including both baryons and dark matter) and the cosmological constant, respectively; ρ_c is the critical density; H_0 is the Hubble parameter at the present time; z is the redshift, and $z_{up} = m_{B_1}/E - 1$ since the maximum energy of photon in the rest frame of annihilation is $E = m_{B_1}$; the term $e^{-z/z_{max}}$ with $z_{max}(E) \sim 3.3(E/10\text{GeV})^{-0.8}$ takes the optical depth into account [46]. For the numerical results, we use [47]

$$\Omega_{B_1} h^2 = 0.1099, \quad \Omega_M h^2 = 0.1326, \quad \Omega_\Lambda = 0.742, \quad \rho_c = 1.0537 \times 10^{-5} \text{GeV/cm}^3. \quad (3.23)$$

On the other hand, the gamma-ray flux from the annihilation of B_1 in the Milky Way halo is

$$\left[E^2 \frac{dJ_\gamma}{dE} \right]_{halo} = \frac{E^2}{4\pi} \frac{1}{2m_{B_1}^2} \frac{dN_\gamma}{dE} \left\langle \int_{los} \rho^2(\vec{\ell}) d\vec{\ell} \right\rangle, \quad (3.24)$$

where ρ_{halo} is the density profile of dark matter in the Milky Way, $\left\langle \int_{los} \rho^2(\vec{\ell}) d\vec{\ell} \right\rangle$ is the average of the integration along the line of sight (los).

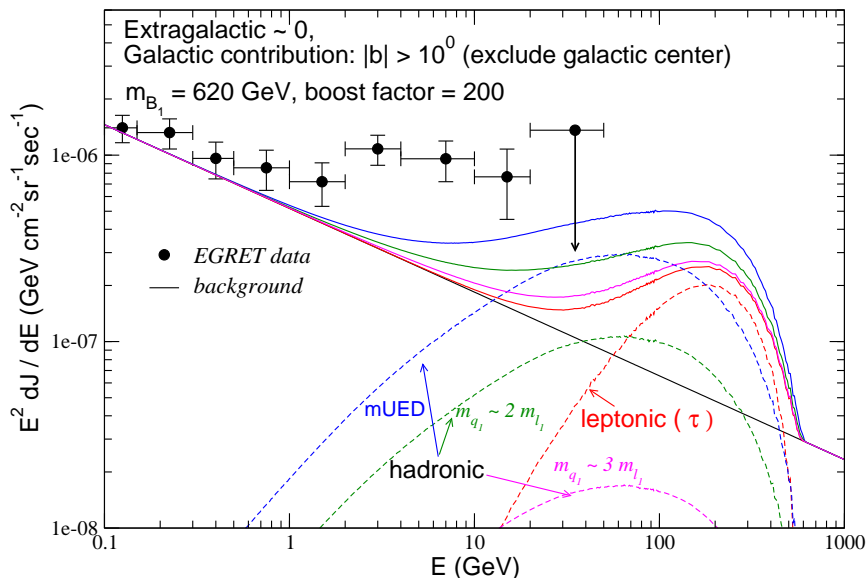


Figure 9. The diffusive gamma-ray predicted in mUED and split-UED models, together with EGRET data. The solid lines are for signals with background, blue line is for mUED; green, magenta and red lines are for $m_{q_1} = 2m_{l_1}$, $m_{q_1} = 3m_{l_1}$ and $m_{q_1} \rightarrow \infty$, respectively. Signals of dark matter annihilation are shown separately in dashed lines for leptonic final state (red), hadronic final states in mUED (blue) and in split-UED with $m_{q_1} = 2m_{l_1}$ (green) and $m_{q_1} = 3m_{l_1}$ (magenta).

Since there are still big uncertainties and ambiguities for modeling the Galaxy center, we integrate over the whole sky except for the zone of the Galactic plane (i.e. exclude the region with the galactic latitudes $|b| < 10^\circ$). For the background, we use a power-law form adopted in ref. [48]

$$\left[E^2 \frac{dJ_\gamma}{dE} \right]_{bg} \simeq 5.18 \times 10^{-7} E^{-0.499} \text{ GeVcm}^{-2}\text{sr}^{-1}\text{sec}^{-1}, \quad (3.25)$$

where E is in units of GeV.

The total flux of diffusive gamma-ray is shown in figure 9, and the signals from the hadronic and leptonic final states in $B_1 B_1$ annihilation are presented as well. We should emphasize that we do not try to fit EGRET data [49, 50] in the plot, since Fermi [13] is expected to have more precise results soon, however, we still show EGRET data for reference. We notice that the extragalactic contribution from cosmological distance is very small even we enhance it by a factor of 10^6 to estimate the effect of subhalo [46]. The gamma-ray in the decay of π^0 from hadron cascade decay is softer than that from the decay of τ , therefore the distribution become flater when more quarks are produced in B_1 annihilation. By suppressing the fraction of the quark mode in the final state, i.e. comparing mUED (blue lines) and split-UED (green, magenta and red lines), the starting point of deviation from the background will shift to high energy⁶ and the predicted peak

⁶The preliminary result of Fermi [51] shows the data is consistent with the estimated background up to $E \sim 10$ GeV, so by enhancing the mass of q_1 in split-UED seems to be preferred, if the preliminary result is thoughtful.

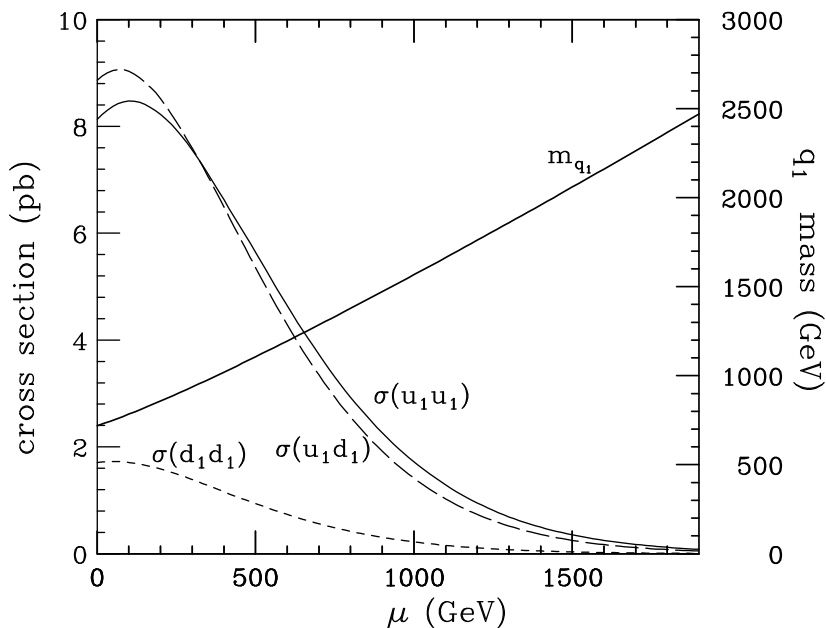


Figure 10. The cross sections and the mass of u_{L1} as functions of the bulk mass μ with fixing $1/R = 620$ GeV. Here, $u_1(d_1)$ includes both u_{L1} and u_{R1} (d_{L1} and d_{R1}) contributions.

at energy about 200 GeV will become smaller. The bump at the high energy is a generic prediction for split-UED even all of the higher order KK quarks are decoupled, because gamma-rays still come from the τ decay, and it can be further examined by the Fermi experiment in the near future.

4 Collider signature of split-UED

Having light colored particles below a few TeV in split-UED, the LHC can produce lots of KK quarks and gluons via QCD interactions. As it is already shown in section 2, one of the features of our model is that KK quarks are split from the other particles, therefore, will lead to collider phenomenology quite different from the mUED models. For example, the 1st KK quark, where we take $m_{q_1} \approx 2m_{B_1}$ through calculations, mainly decays to the 1st KK gluon g_1 and a SM quark, generating at least one high p_T jet due to the big mass gap between q_1 and g_1 . Another one is the existence of tree-level KK number non-conserved interactions between KK-even gauge bosons and the SM fermions, as a result, the production cross sections of 2nd KK gauge bosons can be substantial. It has been shown that the signals of a 2nd KK gluon production can be dominant over the SM background in dijet events after imposing a certain set of cuts at the LHC [9]. In this section, we will focus on the scenarios of 1st KK quarks and gluon, which can only be produced in pairs. The production cross sections involving q_1 at the LHC depend on the bulk mass parameter μ . Among the production cross sections of $q_1 q_1^{(\prime)}$, $q_1 \bar{q}_1^{(\prime)}$ and $\bar{q}_1 \bar{q}_1^{(\prime)}$, the $\sigma(q_1 q_1)$ is dominant one as the valence u and d partons can contribute to the initial states. These productions proceed mainly through the t -channel diagrams with the 1st KK gauge bosons exchanged. The most relevant couplings for these productions are q_1 - q - V_1 , where $V_1 = g_1, B_1$, the 1st

split-UED	mass	SUSY	mass
q_{L1}	1347 GeV	\tilde{u}_L, \tilde{d}_L	1355, 1358 GeV
u_{R1}	1322 GeV	\tilde{u}_R	1304 GeV
d_{R1}	1318 GeV	\tilde{d}_R	1263 GeV
g_1	794 GeV	\tilde{g}	799 GeV
B_1	621 GeV	$\tilde{\chi}_1^0$	622 GeV

Table 4. Mass spectrum of split-UED at $1/R = 620$ GeV and $\mu = 700$ GeV. The corresponding SUSY point generated using ISAJET is also listed.

KK W -boson W_1 and the 1st KK Z -boson Z_1 . The cross section $\sigma(u_1 u_1)$, $\sigma(u_1 d_1)$ and $\sigma(d_1 d_1)$ are plotted in figure 10 with varying μ , and we neglect the $q_1 \bar{q}_1^{(l)}$ productions, since they are insignificant. For small μ , the production cross sections increase with increasing μ due to the enhancement from the couplings, as shown in figure 3, since the cross section is proportional to $(\mathcal{G}_{110})^4$. For large μ , on the other hand, those cross sections decrease very quickly with increasing μ (increasing m_{q_1}) as expected. For the $g_1 q_1$ and $g_1 g_1$ productions, the cross sections, which are not shown, are at the same order as that of $q_1 q_1$. Here all cross sections are calculated using CalcHEP [52] by modifying the mUED model file in ref. [53].

The signature of split-UED $q_1 \bar{q}_1$ productions followed by $q_1 \rightarrow g_1 q \rightarrow B_1 q X$ is two high p_T jets plus soft jets/leptons and large missing momentum. The kinematics and the decay branching ratios are very similar to those of the corresponding supersymmetric model (SUSY) processes, namely the $\tilde{q}\tilde{q}$ productions followed by $\tilde{q} \rightarrow \tilde{g} q \rightarrow \tilde{\chi}_1^0 q X$ with squark mass $m_{\tilde{q}} = m_{q_1}$, gluino mass $m_{\tilde{g}} = m_{g_1}$ and the lightest neutralino mass $m_{\tilde{\chi}_1^0} = m_{B_1}$. Therefore, we mimic split-UED collider signatures of q_1 pair productions at the LHC by scaling the total cross sections of SUSY signatures with the model point whose mass spectrum is similar to that of the split-UED. Furthermore, because collider signatures of $q_1 \bar{q}_1$ are the same as that of $\tilde{q}\tilde{q}$, they share the same SM background. Since the SM background for squark and gluino productions at the LHC is very well studied [54], we apply the same cuts in our calculation. The model points we study are listed in table 4, in which we use ISAJET [55] for SUSY, and we take $1/R$ and μ to be 620 GeV and 700 GeV, respectively, for split-UED so that $m_{q_1} \approx 2m_{B_1}$. The events are generated by using HERWIG [56] for SUSY processes, then we regard them as the split-UED events, and detector simulations are carried out by AcerDET [57]. Table 5 shows the acceptances of the events after imposing the following basic cuts:

$$M_{\text{eff}} > 500 \text{ GeV}, \quad E_{T_{\text{miss}}} > \max(100 \text{ GeV}, 0.2M_{\text{eff}}), \quad n_{100} \geq 1, \quad n_{50} \geq 4, \quad (4.1)$$

M_{eff} is the scalar sum of the p_T of the first four leading jets; $E_{T_{\text{miss}}}$ is the transverse missing momentum; n_{100} (n_{50}) is the number of jets with $p_T > 100$ (50) GeV. Furthermore, we also use harder cuts on M_{eff} with $M_{\text{eff}} > 1, 1.5\text{TeV}$.

We can see that the acceptance is about 40 % for q_1 pair production after the basic cuts. On the other hand, the efficiency to select the g_1 pair production is much smaller, especially when a large M_{eff} is required. For example, the number of events from the 1st KK gluon

	after standard cut	$M_{\text{eff}} > 1 \text{ TeV}$	$M_{\text{eff}} > 1.5 \text{ TeV}$
$q_1 q_1$	0.40	0.37	0.21
$q_1 g_1$	0.30	0.18	0.049
$g_1 g_1$	0.18	0.04	0.007

Table 5. The acceptances for the split-UED $q_1 q_1$, $q_1 g_1$ and $g_1 g_1$ productions after imposing basic event selection cuts (4.1) and harder M_{eff} cuts for the model point in table 4. Note that these numbers are obtained from SUSY events.

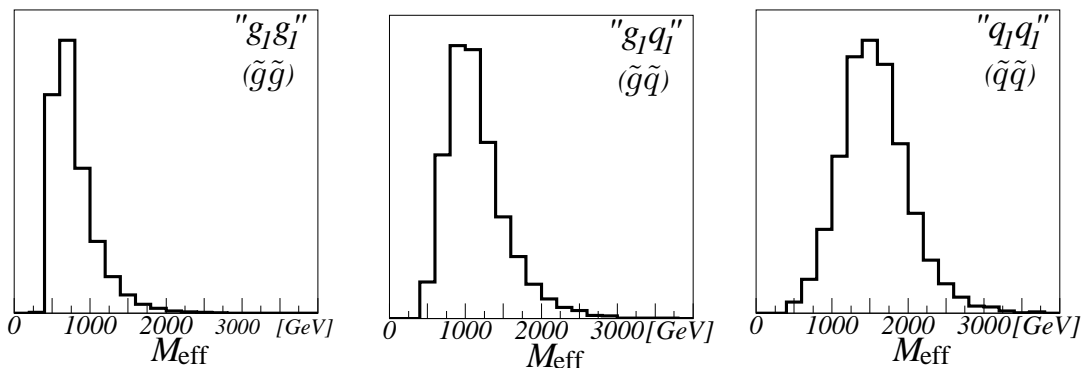


Figure 11. M_{eff} distributions for “ $g_1 g_1$ ”, “ $q_1 g_1$ ” and “ $q_1 q_1$ ” from left to right obtained by corresponding SUSY channels $\tilde{g}\tilde{g}$, $\tilde{q}\tilde{g}$ and $\tilde{q}\tilde{q}$. We neglect the y-axis here since we focus on the shapes, and we see that the distributions shift to higher energy region from left to right.

pair production reduces by factor of 1/30 after imposing the basic cuts with $M_{\text{eff}} > 1 \text{ TeV}$. This is because the probability of having high p_T jets and large E_{Tmiss} is very low for the g_1 production events at our point. Thus, we expect $g_1 g_1$ production is not promising due to the very small efficiency found in the simulation. The $g_1 q_1$ production may be easier to detect compared to the $g_1 g_1$ case with the help of the high p_T jet from $q_1 \rightarrow q g_1$, although the signal and the background separation would be worse compared with $q_1 q_1$ production. Therefore we only consider $q_1 q_1$ productions in the following studies. For completeness, we show the M_{eff} distributions for $g_1 g_1$, $q_1 g_1$ and $q_1 q_1$ in figure 14. Again these results are obtained from SUSY events mimicking split-UED with the same kinematics. The total production cross section of $q_1 q_1$, including $u_{L1}, d_{L1}, u_{R1}, d_{R1}$, is 7.64 pb, and we expect 7640 events for 1 fb^{-1} . According to table 14, we expect $7640 \times 0.37 = 2830$ events left under the standard cut with $M_{\text{eff}} > 1 \text{ TeV}$. We should also consider lepton veto before using the background studied in ref. [54]. Although it depends on the lepton branching ratio, we expect more than a half number of events, i.e. 1400, remain with the lepton veto. The number of SM background events with the same cut for 1 fb^{-1} is less than 300 according to the M_{eff} distribution shown in ref. [54]. Therefore the $q_1 q_1$ signal distribution is well above the background distribution for $M_{\text{eff}} > 1000 \text{ GeV}$. Given the enough statistics, we now discuss the possibility to determine some of the split-UED particle masses. Figure 12 shows the M_{T2} [58] distribution of the two highest p_T jets

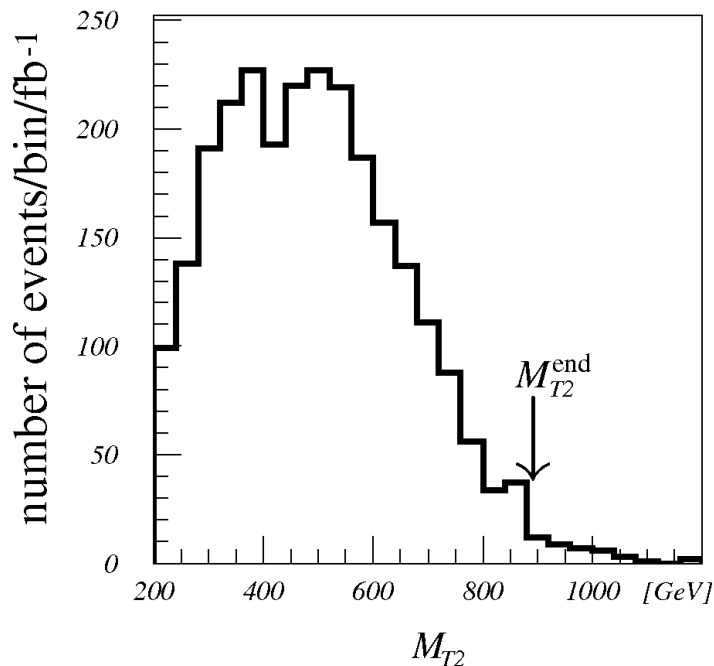


Figure 12. The M_{T2} distribution for $q_1 q_1$ production events under the standard cut with $M_{\text{eff}} > 1 \text{ TeV}$ for 1 fb^{-1} . We can see that the end point of M_{T2} distribution is given by $m_{q_1} - \frac{m_{g_1}^2}{m_{q_1}} \simeq 880 \text{ GeV}$. The bin size is 10 GeV/bin . Note that we do not apply any lepton veto cut for this plot.

under the standard cut with $M_{\text{eff}} > 1000 \text{ GeV}$. The M_{T2} is usually used to determine the masses of unknown particles which are pair-produced and decay identically. In our case, we have two q_1 's being produced, and both decay into $g_1 q$. Here the M_{T2} is calculated from the two highest p_T jets, j_1 and j_2 and a missing transverse momentum defined as $p_{T\text{miss}} = -p_{Tj_1} - p_{Tj_2}$ and the formula is

$$M_{T2} = \min_{p_{T\text{miss}}=q_{T1}+q_{T2}} [\max\{M_T(q_{T1}, p_{j_1}, m_{\text{trial}}), M_T(q_{T2}, p_{j_2}, m_{\text{trial}})\}], \quad (4.2)$$

where q_{T1} and q_{T2} are two dummy parameters that make up $p_{T\text{miss}}$, and the minimization is taken for all possible sets of q_{T1} and q_{T2} ; $p_{j_1(j_2)}$ is the momentum of $j_{1(2)}$; m_{trial} is the trial mass that represents the unknown mass of the daughter particle (g_1 in our process) and M_T is the transverse mass. The M_{T2} depends on the trial mass m_{trial} , and we took $m_{\text{trial}} = 0$ in figure 12. For our simulation, the two highest p_T jets comes from $q_1 \rightarrow g_1 q$, and the end point of M_{T2} should be m_{q_1} when the trial particle mass m_{trial} is taken as the true mass of g_1 . Another important fact is that when there are no initial state radiations, the formula of the M_{T2} endpoint for $m_{\text{trial}} = 0$ has a general form given as

$$M_{T2}^{\text{end}} = m_A - \frac{m_X^2}{m_A}, \quad (4.3)$$

where m_A is the mass of mother particle which is pair produced and m_X is the mass of the unknown daughter particle, and in our case $m_A = m_{q_1}$ and $m_X = m_{g_1}$. We can see that the

M_{T2} distribution in figure 12 has a clear end point which is consistent with the predicted value $M_{T2}^{\text{end}} \simeq 880$ GeV for the model point in table 4. Although we are unable to measure precise masses of q_1 and g_1 , we still have a useful information on their combination.

Finally, let us comment on the comparison with mSUGRA. If we assume the signature comes from squark production, with a typical mass spectrum $m_{\tilde{q}} \sim 1$ TeV and gives the similar M_{T2} end point, the cross section is much smaller than that of the split-UED point. Thus, SUSY and split-UED should be distinguished based on the event rates, although the kinematical nature of the signal is similar. We can get a rough understanding on the enhancement of the cross section in split-UED by comparing the helicity structure of squarks/gluinos and corresponding KK quarks/gluons [8].⁷

5 Conclusion

The split-UED model proposed in ref. [9] is studied in detail. From the basic set-up of the model, we calculate all the masses (including one-loop radiative corrections to the masses) and relevant couplings for the first KK particles. Characteristic split spectrum of KK quark states is realized and enables us to control the hadronic branching fraction of the LKP annihilation by one parameter, bulk mass scale (μ). In the non-relativistic limit, such a branching fraction decreases very fast by increasing μ .

In order to explain the anomalies from the cosmic ray, we fixed the size of extra dimension ($1/R \simeq 620$ GeV) from the peak position in flux of electrons plus positrons observed by ATIC and PPB-BETS, with boost factor $B = 200$. Then all data from PAMELA, ATIC, and PPB-BETS can simultaneously be fitted very well. It is important to notice that such a dark matter mass in split-UED generically can explain the right amount of relic density of dark matter ($\Omega \simeq 0.23$). To avoid all the strong constraints known up to date, we take $m_{q_1} \gtrsim 2/R$ so that the hadronic branching fraction of LKP annihilation is significantly smaller than the leptonic one ($\sigma_{q\bar{q}}/\sigma_{l\bar{l}} < 10\%$) and the cosmic antiproton flux is suppressed more than the safe rate. The flux of cosmic gamma-rays from pion decay is also highly suppressed and hardly detected in low energy region ($E_\gamma \lesssim 20$ GeV). However future coverage of high energy domain in $O(100)$ GeV will make it possible to detect gamma-rays originated by tau lepton which is still sizable.

At the LHC, the 1st KK colored particles (KK quarks and gluons) in split-UED are copiously produced and further decay into hard jets, soft jets/leptons and dark matter (missing energy). Because of the large mass splitting between the 1st KK quark q_1 and 1st KK gluon g_1 , we can separate out the production of $g_1 g_1$, $g_1 q_1$ and $q_1 q_1$ by using the M_{eff} cuts. We focus on the $q_1 q_1$ production, in particular, which has two hard jets so that we can distinguish the signals from the SM background. The split-UED q_1 pair signal is simulated by scaling the SUSY signatures with the same mass spectrum. After the appropriate cuts, our signal is well above the SM background. We calculate the M_{T2} distribution of the q_1 pair signals, and its end point reflects the information for combination of q_1 and g_1 masses. Although we are unable to determine the mass of individual particle in split-UED, its predictions of the signatures of $q_1 q_1$ production at the LHC, e.g. M_{eff} and M_{T2} , can be

⁷See also [59] for similar phenomenon in Little Higgs model.

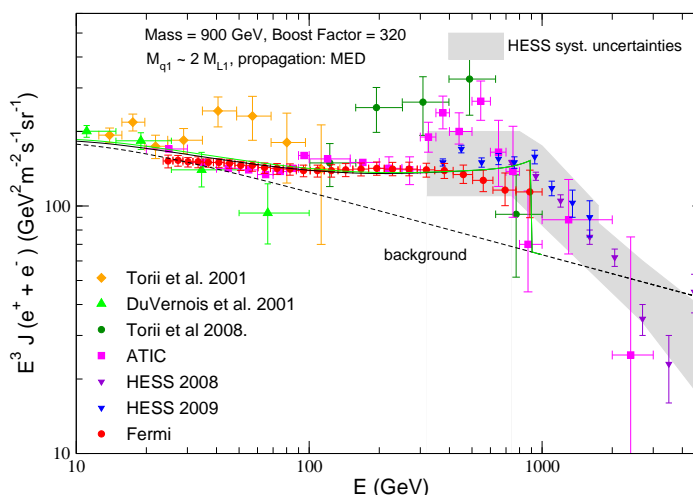


Figure 13. The flux of electron plus positron from LKP dark matter annihilation using MED diffusion model, compared with experimental data including the Fermi-LAT [60] and HESS [61] data.

examined whether they are consistent with the cosmic-ray signatures in the near future, and vice versa.

6 Note added

After completion of the current work, the Fermi-LAT experiment reported new measurements of the spectrum of cosmic-ray electrons-plus-positrons between 20 GeV and 1TeV [60]. The prominent spectral feature observed by ATIC was not confirmed by the new Fermi data but still a sizable excess was seen in high energy region. Combining the significant spectral steeping at high energy observed by the HESS [61], a heavier dark matter is required to account for the anomalies in cosmic ray electron [62]. In figure 13 we show the split-UED fit to Fermi data as well as PAMELA data assuming a 900 GeV KK dark matter.⁸ Having a larger mass we need to have a bit larger boost factor about 320 though.

If the LKP ($\sim 1/R$) becomes heavier, KK quarks become heavier accordingly so that their production cross sections get smaller. We show the production cross sections of KK quark pairs taking $1/R = 900\text{GeV}$ in the figure 14. With $\mu_5 \simeq 1/R = 900\text{GeV}$, as is required to make the hadronic branching fraction small enough, we have $m_{q_1} = 1153\text{GeV}$ and $M_{u_1} = 1846\text{GeV}$ and $\sigma(q_1 q_1) = 0.95\text{pb}$. Even in the case, still the signal is expected to be seen over the SM backgrounds.

⁸We can add very small 5D bulk mass terms for leptons, then a LKP with 900 GeV mass would produce the right relic density without coannihilation [11].

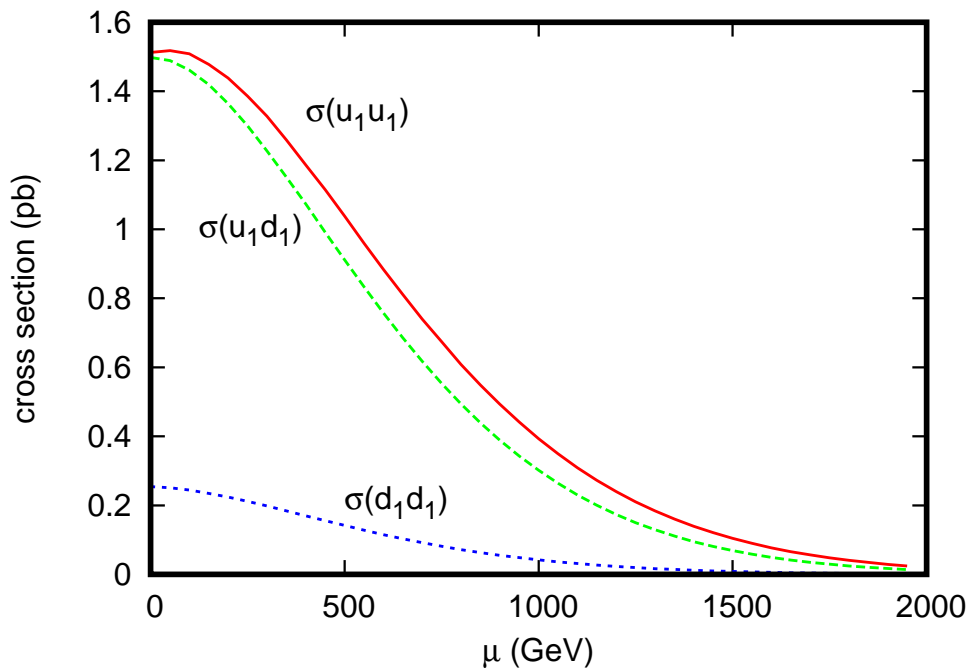


Figure 14. The cross sections as functions of the bulk mass μ with fixing $1/R = 900$ GeV. Here, $u_1(d_1)$ includes both u_{L1} and u_{R1} (d_{L1} and d_{R1}) contributions.

Acknowledgments

C.R.C. thanks F. Takahashi for useful discussions. This work was supported by the World Premier International Research Center Initiative (WPI initiative) by MEXT, Japan.

A KK decomposition in split-UED

For all the gauge bosons, scalars, and leptons, their KK decompositions are the same as those in mUED. For bosons and fermions that are in the same chirality of the zero mode, which has $(+, +)$ boundary condition at $[-L, L]$, the KK decomposition is:

$$\Phi_+(y) = \frac{1}{\sqrt{2L}}\phi_0(x) + \frac{1}{\sqrt{L}} \sum_{n^+, n^-} \sin\left[\frac{n^- \pi}{2L}y\right] \phi_{n^-}(x) + \cos\left[\frac{n^+ \pi}{2L}y\right] \phi_{n^+}(x). \quad (\text{A.1})$$

While for fermions that are in the opposite chirality of the zero mode, which has the $(-, -)$ boundary condition at $[-L, L]$, the KK decomposition is:

$$\Phi_-(y) = \frac{1}{\sqrt{L}} \sum_{n^+, n^-} \cos\left[\frac{n^- \pi}{2L}y\right] \phi_{n^-}(x) + \sin\left[\frac{n^+ \pi}{2L}y\right] \phi_{n^+}(x). \quad (\text{A.2})$$

The label n^- or n^+ here stands for the n -th KK modes with the even/odd KK parity.⁹

⁹In our convention, the KK number $n^- = 2n^- - 1$ and $n^+ = 2n^+$ for the $\{n^-, n^+\}$ in ref. [14].

For the quark, we consider the case in which a SM quark is embedded into $\Psi_+ = P_+ \Psi$ component of a 5D Dirac fermion Ψ , where $P_+ = (1 + \gamma_5)/2$ is the positive chirality projection operator. The other case could be considered quite similarly by replacing μ by $-\mu$. A convenient way of expressing the KK decomposition is in the form [9, 14]:

$$\begin{aligned}\Psi_+(x, y) &= \sum_{n^+, n^-} g_{n^+}(|y|)\chi_{n^+}(x) + \epsilon(y)g_{n^-}(|y|)\chi_{n^-}(x), \\ \Psi_-(x, y) &= \sum_{n^+, n^-} \epsilon(y)f_{n^+}(|y|)\psi_{n^+}(x) + f_{n^-}(|y|)\psi_{n^-}(x).\end{aligned}\tag{A.3}$$

The 5D profiles satisfy the following coupled, first-order equations of motion

$$\begin{aligned}\partial_y g_n + \mu g_n - m_n f_n &= 0, \\ \partial_y f_n - \mu f_n + m_n g_n &= 0,\end{aligned}\tag{A.4}$$

with each 5D profile $g_{n^+}, g_{n^-}, f_{n^+}, f_{n^-}$ satisfying the $(+, +), (-, +), (-, -), (+, -)$ boundary condition at $y = 0$ and L , respectively. Once the solution for $y \in [0, L]$ is obtained, the solution to the whole space is determined from eq. (A.3) thanks to the symmetry.

For the zero modes, $m_n = 0$, the equations are separable and the solution is given as

$$g_{0^+}(y) = A_0 \exp\left(\int_0^y \lambda(\Phi(s)) ds\right) = A_0 \exp(\mu y),\tag{A.5}$$

with the normalization factor $A_0 = \sqrt{\mu/e^{(2\mu L-1)}}$. There is no zero mode company for g_{0^+} but each of the KK modes has its couple and fill the spinor states of the Dirac spinor. The solution for the even KK modes is

$$\begin{aligned}g_{n^+} &= \sqrt{\frac{1}{L}} \left[\frac{k_{n^+}}{m_{n^+}} \cos(k_{n^+} y) + \frac{\mu}{m_{n^+}} \sin(k_{n^+} y) \right], \\ f_{n^+} &= -\sqrt{\frac{1}{L}} \sin(k_{n^+} y),\end{aligned}\tag{A.6}$$

where the KK mass $m_{n^+} = \sqrt{\mu^2 + k_{n^+}^2}$ and $k_{n^+} = n\pi/L$ ($n \in \mathcal{Z}$).

To avoid the very light 1st KK quark, we choose $\mu > 0$ and the zero mode is quasi-localized at the boundary $y = \pm L$. For odd KK modes, the solution is

$$\begin{aligned}g_{n^-} &= -\sqrt{\frac{1}{L}} \sin(k_{n^-} y), \\ f_{n^-} &= \sqrt{\frac{1}{L}} \left[\frac{k_{n^-}}{m_{n^-}} \cos(k_{n^-} y) + \frac{\mu}{m_{n^-}} \sin(k_{n^-} y) \right],\end{aligned}\tag{A.7}$$

where the KK mass $m_n = \sqrt{\mu^2 + k_n^2}$ and k_n is the n -th solution of the equation

$$k_{n^-} = -\mu \tan(k_{n^-} L).\tag{A.8}$$

When μ increases from 0 to $+\infty$, k_{n^-} increases from $(n - 1/2)\pi/L$ to $n\pi/L$. In this case, in the limit of $\mu \rightarrow +\infty$, all KK modes could be decoupled.

References

- [1] PAMELA collaboration, O. Adriani et al., *An anomalous positron abundance in cosmic rays with energies 1.5-100 GeV*, *Nature* **458** (2009) 607 [[arXiv:0810.4995](#)] [[SPIRES](#)].
- [2] J. Chang et al., *An excess of cosmic ray electrons at energies of 300-800 GeV*, *Nature* **456** (2008) 362 [[SPIRES](#)].
- [3] PPB-BETS collaboration, S. Torii et al., *High-energy electron observations by PPB-BETS flight in Antarctica*, [arXiv:0809.0760](#) [[SPIRES](#)].
- [4] D. Hooper, P. Blasi and P.D. Serpico, *Pulsars as the sources of high energy cosmic ray positrons*, *JCAP* **01** (2009) 025 [[arXiv:0810.1527](#)] [[SPIRES](#)];
H. Yuksel, M.D. Kistler and T. Stanev, *TeV gamma rays from Geminga and the origin of the GeV positron excess*, *Phys. Rev. Lett.* **103** (2009) 051101 [[arXiv:0810.2784](#)] [[SPIRES](#)].
- [5] C.-R. Chen, F. Takahashi and T.T. Yanagida, *Gamma rays and positrons from a decaying hidden gauge boson*, *Phys. Lett. B* **671** (2009) 71 [[arXiv:0809.0792](#)] [[SPIRES](#)];
C.-R. Chen and F. Takahashi, *Cosmic rays from leptonic dark matter*, *JCAP* **02** (2009) 004 [[arXiv:0810.4110](#)] [[SPIRES](#)];
I. Cholis, D.P. Finkbeiner, L. Goodenough and N. Weiner, *The PAMELA positron excess from annihilations into a light boson*, [arXiv:0810.5344](#) [[SPIRES](#)];
P.-f. Yin et al., *PAMELA data and leptonically decaying dark matter*, *Phys. Rev. D* **79** (2009) 023512 [[arXiv:0811.0176](#)] [[SPIRES](#)];
K. Ishiwata, S. Matsumoto and T. Moroi, *Cosmic-ray positron from superparticle dark matter and the PAMELA anomaly*, *Phys. Lett. B* **675** (2009) 446 [[arXiv:0811.0250](#)] [[SPIRES](#)];
A. Ibarra and D. Tran, *Decaying dark matter and the PAMELA anomaly*, *JCAP* **02** (2009) 021 [[arXiv:0811.1555](#)] [[SPIRES](#)];
C.-R. Chen, M.M. Nojiri, F. Takahashi and T.T. Yanagida, *Decaying hidden gauge boson and the PAMELA and ATIC/PPB-BETS anomalies*, [arXiv:0811.3357](#) [[SPIRES](#)];
E. Nardi, F. Sannino and A. Strumia, *Decaying dark matter can explain the e^\pm excesses*, *JCAP* **01** (2009) 043 [[arXiv:0811.4153](#)] [[SPIRES](#)];
K. Hamaguchi, S. Shirai and T.T. Yanagida, *Cosmic ray positron and electron excess from hidden-fermion dark matter decays*, *Phys. Lett. B* **673** (2009) 247 [[arXiv:0812.2374](#)] [[SPIRES](#)];
F. Takahashi and E. Komatsu, *Gravitational dark matter decay and the ATIC/PPB-BETS excess*, [arXiv:0901.1915](#) [[SPIRES](#)];
K. Hamaguchi, F. Takahashi and T.T. Yanagida, *Decaying gravitino dark matter and an upper bound on the gluino mass*, *Phys. Lett. B* **677** (2009) 59 [[arXiv:0901.2168](#)] [[SPIRES](#)];
C.-H. Chen, C.-Q. Geng and D.V. Zhuridov, *ATIC/PAMELA anomaly from fermionic decaying Dark Matter*, [arXiv:0901.2681](#) [[SPIRES](#)];
X. Chen, *Decaying hidden dark matter in warped compactification*, [arXiv:0902.0008](#) [[SPIRES](#)];
B. Kyae, *PAMELA/ATIC anomaly from the meta-stable extra dark matter component and the leptophilic Yukawa interaction*, *JCAP* **07** (2009) 028 [[arXiv:0902.0071](#)] [[SPIRES](#)];
K.J. Bae and B. Kyae, *PAMELA/ATIC anomaly from exotic mediated dark matter decay*, *JHEP* **05** (2009) 102 [[arXiv:0902.3578](#)] [[SPIRES](#)].
- [6] L. Bergstrom, T. Bringmann and J. Edsjo, *New positron spectral features from supersymmetric dark matter - a way to explain the PAMELA data?*, *Phys. Rev. D* **78** (2008) 103520 [[arXiv:0808.3725](#)] [[SPIRES](#)];

- M. Cirelli and A. Strumia, *Minimal dark matter predictions and the PAMELA positron excess*, [arXiv:0808.3867](#) [SPIRES];
- V. Barger, W.Y. Keung, D. Marfatia and G. Shaughnessy, *PAMELA and dark matter*, *Phys. Lett. B* **672** (2009) 141 [[arXiv:0809.0162](#)] [SPIRES];
- I. Cholis, L. Goodenough, D. Hooper, M. Simet and N. Weiner, *High energy positrons from annihilating dark matter*, [arXiv:0809.1683](#) [SPIRES];
- M. Cirelli, M. Kadastik, M. Raidal and A. Strumia, *Model-independent implications of the e^\pm , \bar{p} cosmic ray spectra on properties of dark matter*, *Nucl. Phys. B* **813** (2009) 1 [[arXiv:0809.2409](#)] [SPIRES];
- J.-H. Huh, J.E. Kim and B. Kyae, *Two dark matter components in $N_{DM}MSSM$ and PAMELA data*, *Phys. Rev. D* **79** (2009) 063529 [[arXiv:0809.2601](#)] [SPIRES];
- N. Arkani-Hamed and N. Weiner, *LHC signals for a superUnified theory of dark matter*, *JHEP* **12** (2008) 104 [[arXiv:0810.0714](#)] [SPIRES];
- I. Cholis, D.P. Finkbeiner, L. Goodenough and N. Weiner, *The PAMELA positron excess from annihilations into a light boson*, [arXiv:0810.5344](#) [SPIRES];
- Y. Nomura and J. Thaler, *Dark matter through the axion portal*, *Phys. Rev. D* **79** (2009) 075008 [[arXiv:0810.5397](#)] [SPIRES];
- R. Harnik and G.D. Kribs, *An effective theory of dirac dark matter*, *Phys. Rev. D* **79** (2009) 095007 [[arXiv:0810.5557](#)] [SPIRES];
- D. Feldman, Z. Liu and P. Nath, *PAMELA positron excess as a signal from the hidden sector*, *Phys. Rev. D* **79** (2009) 063509 [[arXiv:0810.5762](#)] [SPIRES];
- Y. Bai and Z. Han, *A unified dark matter model in sUED*, *Phys. Rev. D* **79** (2009) 095023 [[arXiv:0811.0387](#)] [SPIRES];
- I. Cholis, G. Dobler, D.P. Finkbeiner, L. Goodenough and N. Weiner, *The case for a 700+ GeV WIMP: cosmic ray spectra from ATIC and PAMELA*, [arXiv:0811.3641](#) [SPIRES];
- P.J. Fox and E. Poppitz, *Leptophilic dark matter*, *Phys. Rev. D* **79** (2009) 083528 [[arXiv:0811.0399](#)] [SPIRES];
- G. Bertone, M. Cirelli, A. Strumia and M. Taoso, *Gamma-ray and radio tests of the e^\pm excess from DM annihilations*, *JCAP* **03** (2009) 009 [[arXiv:0811.3744](#)] [SPIRES];
- K.M. Zurek, *Multi-component dark matter*, *Phys. Rev. D* **79** (2009) 115002 [[arXiv:0811.4429](#)] [SPIRES];
- J. Hisano, M. Kawasaki, K. Kohri and K. Nakayama, *Neutrino signals from annihilating/decaying dark matter in the light of recent measurements of cosmic ray electron/positron fluxes*, *Phys. Rev. D* **79** (2009) 043516 [[arXiv:0812.0219](#)] [SPIRES];
- J. Zhang et al., *Discriminating different scenarios to account for the cosmic e^\pm excess by synchrotron and inverse compton radiation*, *Phys. Rev. D* **80** (2009) 023007 [[arXiv:0812.0522](#)] [SPIRES];
- R. Allahverdi, B. Dutta, K. Richardson-McDaniel and Y. Santoso, *A supersymmetric $B^- L$ dark matter model and the observed anomalies in the cosmic rays*, *Phys. Rev. D* **79** (2009) 075005 [[arXiv:0812.2196](#)] [SPIRES];
- D. Hooper, A. Stebbins and K.M. Zurek, *Excesses in cosmic ray positron and electron spectra from a nearby clump of neutralino dark matter*, *Phys. Rev. D* **79** (2009) 103513 [[arXiv:0812.3202](#)] [SPIRES];
- K.J. Bae, J.-H. Huh, J.E. Kim, B. Kyae and R.D. Viollier, *White dwarf axions, PAMELA data and flipped-SU(5)*, *Nucl. Phys. B* **817** (2009) 58 [[arXiv:0812.3511](#)] [SPIRES];
- L. Bergstrom, G. Bertone, T. Bringmann, J. Edsjo and M. Taoso, *Gamma-ray and radio constraints of high positron rate dark matter models annihilating into new light particles*, *Phys. Rev. D* **79** (2009) 081303 [[arXiv:0812.3895](#)] [SPIRES];
- C.-R. Chen, K. Hamaguchi, M.M. Nojiri, F. Takahashi and S. Torii, *Dark matter model selection and the ATIC/PPB-BETS anomaly*, *JCAP* **05** (2009) 015 [[arXiv:0812.4200](#)] [SPIRES];

- P. Grajek, G. Kane, D. Phalen, A. Pierce and S. Watson, *Is the PAMELA positron excess winos?*, [arXiv:0812.4555](#) [SPIRES];
- M. Baumgart, C. Cheung, J.T. Ruderman, L.-T. Wang and I. Yavin, *Non-Abelian dark sectors and their collider signatures*, *JHEP* **04** (2009) 014 [[arXiv:0901.0283](#)] [SPIRES];
- I. Gogoladze, R. Khalid, Q. Shafi and H. Yuksel, *CMSSM spectroscopy in light of PAMELA and ATIC*, [arXiv:0901.0923](#) [SPIRES];
- S. Khalil, H.-S. Lee and E. Ma, *Generalized lepton number and dark left-right gauge model*, *Phys. Rev. D* **79** (2009) 041701R [[arXiv:0901.0981](#)] [SPIRES];
- Q.-H. Cao, E. Ma and G. Shaughnessy, *Dark matter: the leptonic connection*, *Phys. Lett. B* **673** (2009) 152 [[arXiv:0901.1334](#)] [SPIRES];
- W.-L. Guo and Y.-L. Wu, *Enhancement of dark matter annihilation via Breit-Wigner resonance*, *Phys. Rev. D* **79** (2009) 055012 [[arXiv:0901.1450](#)] [SPIRES];
- P. Meade, M. Papucci and T. Volansky, *Dark matter sees the light*, [arXiv:0901.2925](#) [SPIRES];
- J. Mardon, Y. Nomura, D. Stolarski and J. Thaler, *Dark matter signals from cascade annihilations*, *JCAP* **05** (2009) 016 [[arXiv:0901.2926](#)] [SPIRES];
- D.J. Phalen, A. Pierce and N. Weiner, *Cosmic ray positrons from annihilations into a new, heavy lepton*, [arXiv:0901.3165](#) [SPIRES];
- J. Hisano, M. Kawasaki, K. Kohri, T. Moroi and K. Nakayama, *Cosmic rays from dark matter annihilation and Big-Bang nucleosynthesis*, *Phys. Rev. D* **79** (2009) 083522 [[arXiv:0901.3582](#)] [SPIRES];
- F. Chen, J.M. Cline and A.R. Frey, *A new twist on excited dark matter: implications for INTEGRAL, PAMELA/ATIC/PPB-BETS, DAMA*, *Phys. Rev. D* **79** (2009) 063530 [[arXiv:0901.4327](#)] [SPIRES];
- H.-S. Goh, L.J. Hall and P. Kumar, *The leptonic higgs as a messenger of dark matter*, *JHEP* **05** (2009) 097 [[arXiv:0902.0814](#)] [SPIRES];
- R. Allahverdi, B. Dutta, K. Richardson-McDaniel and Y. Santoso, *Sneutrino dark matter and the observed anomalies in cosmic rays*, *Phys. Lett. B* **677** (2009) 172 [[arXiv:0902.3463](#)] [SPIRES];
- K. Cheung, P.-Y. Tseng and T.-C. Yuan, *Double-action dark matter, PAMELA and ATIC*, *Phys. Lett. B* **678** (2009) 293 [[arXiv:0902.4035](#)] [SPIRES];
- D.P. Finkbeiner, T.R. Slatyer, N. Weiner and I. Yavin, *PAMELA, DAMA, INTEGRAL and signatures of metastable excited WIMPs*, [arXiv:0903.1037](#) [SPIRES].
- [7] T. Appelquist, H.-C. Cheng and B.A. Dobrescu, *Bounds on universal extra dimensions*, *Phys. Rev. D* **64** (2001) 035002 [[hep-ph/0012100](#)] [SPIRES].
- [8] H.-C. Cheng, K.T. Matchev and M. Schmaltz, *Bosonic supersymmetry? Getting fooled at the CERN LHC*, *Phys. Rev. D* **66** (2002) 056006 [[hep-ph/0205314](#)] [SPIRES].
- [9] S.C. Park and J. Shu, *Split-UED and dark matter*, *Phys. Rev. D* **79** (2009) 091702 [[arXiv:0901.0720](#)] [SPIRES].
- [10] G. Servant and T.M.P. Tait, *Is the lightest Kaluza-Klein particle a viable dark matter candidate?*, *Nucl. Phys. B* **650** (2003) 391 [[hep-ph/0206071](#)] [SPIRES].
- [11] K. Kong and K.T. Matchev, *Precise calculation of the relic density of KK dark matter in universal extra dimensions*, *JHEP* **01** (2006) 038 [[hep-ph/0509119](#)] [SPIRES].
- F. Burnell and G.D. Kribs, *The abundance of Kaluza-Klein dark matter with coannihilation*, *Phys. Rev. D* **73** (2006) 015001 [[hep-ph/0509118](#)] [SPIRES].
- [12] O. Adriani et al., *A new measurement of the antiproton-to-proton flux ratio up to 100 GeV in the cosmic radiation*, *Phys. Rev. Lett.* **102** (2009) 051101 [[arXiv:0810.4994](#)] [SPIRES].

- [13] FERMI GAMMA-RAY SPACE TELESCOPE (FORMERLY GLAST) collaboration, see the webpage: <http://fermi.gsfc.nasa.gov/>.
- [14] K. Agashe, A. Falkowski, I. Low and G. Servant, *KK parity in warped extra dimension*, *JHEP* **04** (2008) 027 [[arXiv:0712.2455](#)] [[SPIRES](#)];
- [15] D. Hooper and K.M. Zurek, *The PAMELA and ATIC signals from Kaluza-Klein dark matter*, *Phys. Rev. D* **79** (2009) 103529 [[arXiv:0902.0593](#)] [[SPIRES](#)].
- [16] T. Flacke, A. Menon and D.J. Phalen, *Non-minimal universal extra dimensions*, *Phys. Rev. D* **79** (2009) 056009 [[arXiv:0811.1598](#)] [[SPIRES](#)].
- [17] H.-C. Cheng, K.T. Matchev and M. Schmaltz, *Radiative corrections to Kaluza-Klein masses*, *Phys. Rev. D* **66** (2002) 036005 [[hep-ph/0204342](#)] [[SPIRES](#)].
- [18] T. Sjöstrand, S. Mrenna and P. Skands, *PYTHIA 6.4 physics and manual*, *JHEP* **05** (2006) 026 [[hep-ph/0603175](#)] [[SPIRES](#)].
- [19] L. Bergstrom, P. Ullio and J.H. Buckley, *Observability of gamma rays from dark matter neutralino annihilations in the Milky Way halo*, *Astropart. Phys.* **9** (1998) 137 [[astro-ph/9712318](#)] [[SPIRES](#)].
- [20] J. Hisano, S. Matsumoto, O. Saito and M. Senami, *Heavy Wino-like neutralino dark matter annihilation into antiparticles*, *Phys. Rev. D* **73** (2006) 055004 [[hep-ph/0511118](#)] [[SPIRES](#)].
- [21] D. Maurin, F. Donato, R. Taillet and P. Salati, *Cosmic rays below $Z = 30$ in a diffusion model: new constraints on propagation parameters*, *Astrophys. J.* **555** (2001) 585 [[astro-ph/0101231](#)] [[SPIRES](#)].
- [22] T. Delahaye, R. Lineros, F. Donato, N. Fornengo and P. Salati, *Positrons from dark matter annihilation in the galactic halo: theoretical uncertainties*, *Phys. Rev. D* **77** (2008) 063527 [[arXiv:0712.2312](#)] [[SPIRES](#)].
- [23] I.V. Moskalenko and A.W. Strong, *Production and propagation of cosmic-ray positrons and electrons*, *Astrophys. J.* **493** (1998) 694 [[astro-ph/9710124](#)] [[SPIRES](#)].
- [24] E.A. Baltz and J. Edsjo, *Positron propagation and fluxes from neutralino annihilation in the halo*, *Phys. Rev. D* **59** (1998) 023511 [[astro-ph/9808243](#)] [[SPIRES](#)].
- [25] E.A. Baltz, J. Edsjo, K. Freese and P. Gondolo, *The cosmic ray positron excess and neutralino dark matter*, *Phys. Rev. D* **65** (2002) 063511 [[astro-ph/0109318](#)] [[SPIRES](#)].
- [26] M.A. DuVernois et al., *Cosmic ray electrons and positrons from 1-GeV to 100-GeV: measurements with HEAT and their interpretation*, *Astrophys. J.* **559** (2001) 296 [[SPIRES](#)].
- [27] S. Torii et al., *The energy spectrum of cosmic ray electrons from 10-GeV to 100-GeV observed with a highly granulated imaging calorimeter*, *Astrophys. J.* **559** (2001) 973 [[SPIRES](#)].
- [28] J. Diemand, B. Moore and J. Stadel, *Earth-mass dark-matter haloes as the first structures in the early universe*, *Nature*. **433** (2005) 389 [[astro-ph/0501589](#)] [[SPIRES](#)];
J. Diemand, M. Zemp, B. Moore, J. Stadel and M. Carollo, *Cusps in CDM halos: the density profile of a billion particle halo*, *Mon. Not. Roy. Astron. Soc.* **364** (2005) 665 [[astro-ph/0504215](#)] [[SPIRES](#)].
- [29] J. Lavalle, Q. Yuan, D. Maurin and X.J. Bi, *Full calculation of clumpiness boost factors for antimatter cosmic rays in the light of Λ CDM N-body simulation results*, [arXiv:0709.3634](#) [[SPIRES](#)].

- [30] A. Sommerfeld, *Über die beugung und bremsung der elektrone*, *Annalen Phys.* **403** (1931) 257.
- [31] J. Hisano, S. Matsumoto, M.M. Nojiri and O. Saito, *Non-perturbative effect on dark matter annihilation and gamma ray signature from galactic center*, *Phys. Rev. D* **71** (2005) 063528 [[hep-ph/0412403](#)] [[SPIRES](#)].
- [32] N. Arkani-Hamed, D.P. Finkbeiner, T.R. Slatyer and N. Weiner, *A theory of dark matter*, *Phys. Rev. D* **79** (2009) 015014 [[arXiv:0810.0713](#)] [[SPIRES](#)].
- [33] M. Lattanzi and J.I. Silk, *Can the WIMP annihilation boost factor be boosted by the Sommerfeld enhancement?*, *Phys. Rev. D* **79** (2009) 083523 [[arXiv:0812.0360](#)] [[SPIRES](#)].
- [34] E.J. Chun and J.-C. Park, *Dark matter and sub-GeV hidden U(1) in GMSB models*, *JCAP* **02** (2009) 026 [[arXiv:0812.0308](#)] [[SPIRES](#)].
- [35] M. Ibe, H. Murayama and T.T. Yanagida, *Breit-Wigner enhancement of dark matter annihilation*, *Phys. Rev. D* **79** (2009) 095009 [[arXiv:0812.0072](#)] [[SPIRES](#)].
- [36] F. Donato et al., *Antiprotons from spallation of cosmic rays on interstellar matter*, *Astrophys. J.* **563** (2001) 172 [[astro-ph/0103150](#)] [[SPIRES](#)].
- [37] L.C. Tan and L.K. Ng, *Calculation of the equilibrium anti-proton spectrum*, *J. Phys. G* **9** (1983) 227 [[SPIRES](#)].
- [38] M. Cirelli, R. Franceschini and A. Strumia, *Minimal dark matter predictions for galactic positrons, anti-protons, photons*, *Nucl. Phys. B* **800** (2008) 204 [[arXiv:0802.3378](#)] [[SPIRES](#)].
- [39] L.J. Gleeson and W.I. Axford, *Cosmic rays in the interplanetary medium*, *Astrophys. J.* **149** (1967) L115; *Solar modulation of galactic cosmic rays*, *Astrophys. J.* **154** (1968) 1011.
- [40] J.S. Perko, *Solar modulation of galactic antiprotons*, *Astron. Astrophys. J.* **184** (1987) 119.
- [41] E. Nezri, M.H.G. Tytgat and G. Vertongen, *e^+ and \bar{p} from inert doublet model dark matter*, *JCAP* **04** (2009) 014 [[arXiv:0901.2556](#)] [[SPIRES](#)].
- [42] BESS collaboration, S. Orito et al., *Precision measurement of cosmic-ray antiproton spectrum*, *Phys. Rev. Lett.* **84** (2000) 1078 [[astro-ph/9906426](#)] [[SPIRES](#)].
- [43] K. Abe et al., *Measurement of cosmic-ray low-energy antiproton spectrum with the first BESS-Polar Antarctic flight*, *Phys. Lett. B* **670** (2008) 103 [[arXiv:0805.1754](#)] [[SPIRES](#)].
- [44] Y. Asaoka et al., *Measurements of cosmic-ray low-energy antiproton and proton spectra in a transient period of the solar field reversal*, *Phys. Rev. Lett.* **88** (2002) 051101 [[astro-ph/0109007](#)] [[SPIRES](#)].
- [45] WIZARD/CAPRICE collaboration, M. Boezio et al., *The cosmic-ray anti-proton flux between 3-GeV and 49-GeV*, *Astrophys. J.* **561** (2001) 787 [[astro-ph/0103513](#)] [[SPIRES](#)].
- [46] L. Bergstrom, J. Edsjo and P. Ullio, *Spectral gamma-ray signatures of cosmological dark matter annihilations*, *Phys. Rev. Lett.* **87** (2001) 251301 [[astro-ph/0105048](#)] [[SPIRES](#)].
- [47] WMAP collaboration, E. Komatsu et al., *Five-Year Wilkinson Microwave Anisotropy Probe (WMAP1) Observations: Cosmological interpretation*, *Astrophys. J. Suppl.* **180** (2009) 330 [[arXiv:0803.0547](#)] [[SPIRES](#)].
- [48] K. Ishiwata, S. Matsumoto and T. Moroi, *High energy cosmic rays from the decay of gravitino dark matter*, *Phys. Rev. D* **78** (2008) 063505 [[arXiv:0805.1133](#)] [[SPIRES](#)].

- [49] EGRET collaboration, P. Sreekumar et al., *EGRET observations of the extragalactic gamma ray emission*, *Astrophys. J.* **494** (1998) 523 [[astro-ph/9709257](#)] [[SPIRES](#)].
- [50] A.W. Strong, I.V. Moskalenko and O. Reimer, *A new determination of the extragalactic diffuse gamma-ray background from EGRET data*, *Astrophys. J.* **613** (2004) 956 [[astro-ph/0405441](#)] [[SPIRES](#)].
- [51] J. Gudlaugur, *A first look at diffuse galactic emission with Fermi*, talk on behalf of the *Fermi LAT Collaboration*, Long Beach January 2009.
- [52] A. Pukhov, *CalcHEP 3.2: mSSM, structure functions, event generation, batchs and generation of matrix elements for other packages*, [hep-ph/0412191](#) [[SPIRES](#)];
- [53] A. Datta, K. Kong and K.T. Matchev, <http://home.fnal.gov/~kckong/mued/>
- [54] ATLAS collaboration, G. Aad, *Expected performance of the ATLAS experiment detector, trigger, physics*, [CERN-OPEN-2008-020](#) [[arXiv:0901.0512](#)] [[SPIRES](#)].
- [55] F.E. Paige, S.D. Protopopescu, H. Baer and X. Tata, *ISAJET 7.69: a Monte Carlo event generator for pp, $\bar{p}p$ and e^+e^- reactions*, [hep-ph/0312045](#) [[SPIRES](#)].
- [56] G. Corcella et al., *HERWIG 6.5 release note*, [hep-ph/0210213](#) [[SPIRES](#)].
- [57] E. Richter-Was, *AcerDET: a particle level fast simulation and reconstruction package for phenomenological studies on high p_T physics at LHC*, [hep-ph/0207355](#) [[SPIRES](#)].
- [58] A. Barr, C. Lester and P. Stephens, *$m(T2)$: the truth behind the glamour*, *J. Phys. G* **29** (2003) 2343 [[hep-ph/0304226](#)] [[SPIRES](#)].
- [59] K. Kong and S.C. Park, *Phenomenology of top partners at the ILC*, *JHEP* **08** (2007) 038 [[hep-ph/0703057](#)] [[SPIRES](#)].
- [60] THE FERMI LAT collaboration, A.A. Abdo et al., *Measurement of the cosmic ray $e^+ + e^-$ spectrum from 20 GeV to 1 TeV with the Fermi Large Area Telescope*, *Phys. Rev. Lett.* **102** (2009) 181101 [[arXiv:0905.0025](#)] [[SPIRES](#)].
- [61] H.E.S.S. collaboration, F. Aharonian, *Probing the ATIC peak in the cosmic-ray electron spectrum with H.E.S.S.*, [arXiv:0905.0105](#) [[SPIRES](#)].
- [62] THE FERMI LAT collaboration, D. Grasso et al., *On possible interpretations of the high energy electron- positron spectrum measured by the Fermi Large Area Telescope*, [arXiv:0905.0636](#) [[SPIRES](#)].